CryoLetters 47(5), 310 - 339 (2026)

https://doi.org/10.54680/fr26510110112

PERSPECTIVE

CRYOPRESERVATION OF CELL-POPULATED BIOENGINEERED CONSTRUCTS - A ROADMAP FOR CHALLENGES, STRATEGIES, AND TRANSLATION

Vitalii Mutsenko[1,2*], Oleksandr Gryshkov[2], Lothar Lauterboeck[2], Sara Leal Marin[2], Natalia Trufanova [1], Elias Anastassopoulos[3], Lilia Kuleshova[2], Birgit Glasmacher[2] and Alexander Y. Petrenko[1]

[1] Institute for Problems of Cryobiology and Cryomedicine, National Academy of Sciences of Ukraine, Kharkiv, Ukraine
[2] Institute for Multiphase Processes, Leibniz University Hannover, Garbsen, Germany
[3] Department of Environmental Sciences, University of Thessaly, Larissa, Greece
* Corresponding author's E-mail: v.mutsenko@cryonas.org.ua

Abstract

The advancement of cell-populated bioengineered constructs (BECs) has created an ever-increasing demand for effective cryopreservation strategies that guarantee long-term storage without compromising structural integrity or biological function. By allowing constructs to be stored until required, cryopreservation helps align tissue construct unrestricted availability with patient needs and enables regenerative treatments to be initiated on demand. Through the prism of biomaterial properties, this review delves into the historical development and recent progress in the in toto (whole cell-biomaterial construct) cryopreservation of engineered artificial tissues. Particular emphasis is placed on elastic fibrous matrices, alginate-based solid and core-shell constructs, and bulk 3D micro- and macroporous scaffolds, complemented by practical examples from the authors' own research. Beyond these aspects, the review explores methods for recording freezing patterns within cell-free BECs to better characterize thermal events and establish reproducible frameworks with minimal construct-to-construct variability. Finally, this work surveys key regulatory considerations and translational barriers that must be overcome to achieve Good Manufacturing Practice (GMP)-compliant, clinically viable cryopreservation protocols for cell-populated BECs.

Keywords: bioengineered constructs; cell-populated scaffolds; cryobags; cryopreservable hydrogels; cryopreservation; infrared thermography; "in air" slow freezing; tissue engineering.

Abbreviations:

BECs	bioengineered constructs
HA	hydroxyapatite
GMP	Good Manufacturing Practice
DMSO	dimethyl sulfoxide
RBCs	red blood cells
MSCs	mesenchymal stromal cells
VEGF	vascular endothelial growth factor
BM-MSCs	bone marrow-derived MSCs
CPAs	cryoprotective agents
PCL	polycaprolactone

MNPs	magnetic nanoparticles
PLA	polylactic acid
EG	ethylene glycol
LN_2	liquid nitrogen
hMSCs	human MSCs
iPSCs	induced pluripotent stem cells
FBS	fetal bovine serum
HUVECs	human umbilical vein endothelial cells
IIF	intracellular ice formation
FDA	fluorescein diacetate
EB	ethidium bromide
MTT	methyl-thiazolyl-tetrazolium
RPE cells	retinal pigment epithelial cells
PROH	1,2-Propanediol
ECM	extracellular matrix
β-TCP	β-tricalcium phosphate
PVA	polyvinyl alcohol
IRT	infrared thermography
cGMP	current Good Manufacturing Practice
CFR	Code of Federal Regulations
USP	United States Pharmacopeial Convention
CRFs	Controlled-Rate Freezers
SOPs	Standard Operating Procedures
FDA	Food and Drug Administration
EMA	European Medicines Agency

INTRODUCTION

Biomaterials are natural or synthetic materials designed to interact with living tissues, and they are a key component of tissue engineering, which aims to repair or replace damaged tissues using the combination of cells, scaffolds, and biochemical signals (1). Within the field of tissue engineering, cryopreservation is integral to clinical and research applications (2) by enabling the long-term storage and centralized distribution of cells, tissues, and bioengineered constructs (BECs) (3, 4, 5, 6).

In tissue engineering, a scaffold is the basic element that provides a 3D extracellular matrix (ECM)-like artificial niche supporting cell viability, proliferation, differentiation, and secretory functions. Additionally, the microarchitecture and physicochemical properties of scaffolds create the local microenvironment around cells that can protect them during cryopreservation. However, scaffolds can also introduce challenges, including mass and heat transfer limitations that may result in uneven distribution of cryoprotective agents (CPAs) and increase the risk of ice-induced structural damage. Ultimately, all these factors can in turn affect post-thaw cell viability and functional recovery.

Given the heterogeneity of biomaterials, structural designs and cell types used in BECs, integral biomaterial- and cell-specific cryopreservation considerations are crucial to ensure effective functional recovery (7).

Starting from donor-derived or subcultured cells, a reliable and readily available source for the bioengineering of constructs (8, 9, 10, 11, 12, 13), cryopreservation can be applied to:

(i) Scaffold-free engineered tissues (14), organoids (15, 16), spheroids (17, 18), cellular sheets (19), microtissues (20) or multicellular clusters (21);

(ii) Cell-populated engineered or naturally derived scaffolds, requiring functional preservation of both the biomaterial and cellular components (4, 5).

Within this framework, intermediately cryopreserved scaffold-free constructs or preformed tissue precursors could serve as building blocks in the generation of more complex BECs (10, 22, 23, 24, 25, 26). In addition, scaffolds can be used as cryopreservation tools (27) or transplantation vehicles after scaffold-free cryopreservation (28, 29) or both at once (2, 30). Furthermore, cryopreserved tissues can subsequently be entrapped within scaffolds to facilitate their recovery during post-thaw culture (particularly ovarian transplants (31) or spermatogonial stem cell culture (32)). Beyond the above, cryopreserved, cell-populated scaffolds can function as co-culture platforms for the expansion of additional cell types (33).

While cryopreservation of isolated cells (34) and prefabricated matrices [e.g., acellularized scaffolds of cryopreserved tissues (35)] offers some flexibility, additional post-thaw repopulation and construct assembly are still required. A concrete clinical case illustrates the workflow for preparing cryopreserved autologous endothelialized vein allografts, with an average production time of 22 ± 8 d. The process involves autologous vein explantation, in vitro cell cultivation, thawing of the cryopreserved vein, subsequent deendothelialization, and reseeding with autologous venous endothelial cells prior to transplantation (36). Such preoperative workflows that especially rely on the *de novo*

generation of 3D scaffolds rarely align with the strict timing of elective surgical procedures, creating a major clinical bottleneck. BECs cryopreserved *in toto* (as a whole), by contrast, can provide an off-the-shelf, ready-to-implant substitute that eliminates preparation delays and enables personalized regenerative surgery on demand. Furthermore, evidence indicates that in toto cryopreservation of cellularized scaffold-based constructs is more advantageous for specific cell types than preservation as cell suspensions or other tissue precursors (37, 38, 39, 40), although this approach poses greater challenges for other cell populations (11, 41, 42, 43).

In addition, cryopreservation in a ready-to-use format offers a versatile cell-populated biomaterial-based ex vivo platforms for large-scale drug screening (44, 45), disease modelling (46, 47), toxicology and high throughput 3D tissue remodeling studies (48), while also supporting the 3R principles of animal welfare by reducing reliance on animal testing. On the other hand, before the transplantation of a post-thaw BEC (e.g., artificial liver) approaches a clinical reality (49), a great deal of cryopreservation work has to take place including optimization of cryopreservation formats, CPAs and parameters (17, 50, 51, 52 52), upscaling of manufacture (53, 54), examination of *in vivo* performance (55, 56) and GMP compliance (57). The schematic below illustrates the strategic integration of cryopreservation within the tissue engineering pipeline providing a renewable resource of BECs for transplantation (Fig. 1).

There are two primary cryopreservation modes that have been explored for *in toto* BEC cryopreservation: slow freezing and vitrification.

Slow-cooling-based cryopreservation techniques, such as controlled-rate freezing (e.g., with induced ice nucleation), are generally better suited for larger and more mechanically robust BECs (58). Currently, slow cooling has been the most frequently applied technique in this area across the world.

On the other hand, vitrification is a physical process in which cells and solutions transition directly from the liquid phase to an amorphous, glass-like state, while avoiding the formation of crystalline ice (6, 59, 60). Achieving and maintaining a stable amorphous state of cells and the vitrified solution also requires the prevention of devitrification during warming (6, 59, 60). This can be attained at various cooling and warming rates, provided that the final vitrification solution concentration and step durations are appropriately calculated (61). A high solute concentration is generally required to maintain a stable amorphous state. On the whole, vitrification is well-suited for small to moderately sized constructs with highly organized architectures or microvascular structures where uniform permeation of high-concentration CPAs is feasible (62).

Production of BECs is a multifaceted

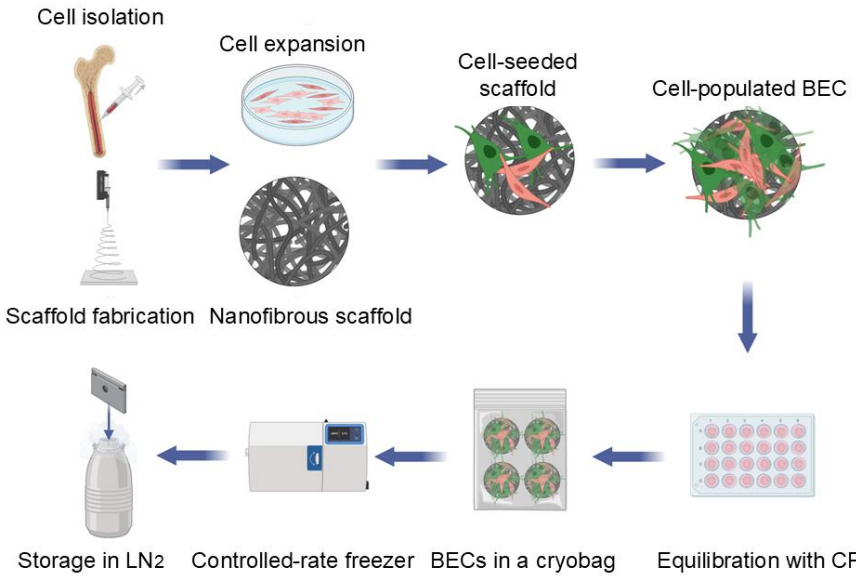

Figure 1. Illustration of the integrated tissue engineering and cryopreservation workflow for cell-populated electrospun scaffolds (Image created in https://BioRender.com).

scientific challenge, with differing approaches to the management of construct production, cryopreservation, and regulatory compliance; for the purpose of this current review, these will be discussed as:

A. Cryopreservation of cell-populated elastic fibrous scaffolds;
B. Encapsulation-mediated cryopreservation using hydrogels, most commonly alginate;
C. Cryopreservation of bulk 3d micro- and macroporous cell-populated scaffolds;
D. Regulatory considerations for translating cryopreservation of becs to clinical applications.

APPROACHES TO THE CRYOPRESERVATION OF CELL-POPULATED ELASTIC FIBROUS SCAFFOLDS

Nanofiber scaffolds are widely used in tissue engineering due to their ability to recapitulate the native ECM topography, supporting cell adhesion, proliferation, and tissue regeneration (63, 64). Concurrently, mechanical resilience of nanofibers provide a valuable system for protecting attached cells from cryo-induced damage in 3D environments.

Kuleshova's research group utilized sterile pouches as a packaging to vitrify polycaprolactone (PCL)-gelatin electrospun scaffolds seeded with porcine mesenchymal stromal cells (MSCs). Their approach involved the gradual addition of low-concentration CPAs and vitrification followed by rapid rewarming and stepwise CPA removal. It merits mention that the structural integrity of the electrospun scaffolds, as well as the metabolic activity, proliferation, and osteogenic differentiation capacity of MSCs, were preserved at levels comparable to non-vitrified control constructs (65).

Later, Costa and colleagues generated fiber meshes based on a starch and PCL blend and seeded them with goat bone marrow stem cells. After 7 d in culture, the bioconstructs were cryopreserved by slow freezing in a cryomedium containing 10% DMSO. The study demonstrated that porous scaffolds exhibited substantially higher post-thaw cell retention and viability than cells grown on non-porous discs discs made from the same material (66). Using silk nanofibrous scaffolds as a cell-support matrix and a high-density polypropylene sterile pouch as a freezing container, Bissoyi et al. preserved umbilical cord-derived MSCs through controlled-rate freezing at 1 °C/min with a cryoprotective mixture of natural osmolytes and 2.5% DMSO. Importantly, post-thaw MSCs viability and differentiation ability as well as mechanical integrity of the scaffolds remained uncompromised (67).

Temperature-responsive electrospun nanofiber meshes made of N-isopropylacrylamide (PNIPAAm), designed by Maeda et al., were explored for the cryopreservation of normal human dermal fibroblasts (68). Cells entrapped within the nanofiber mesh exhibited significantly higher post-thaw viability at 10% and 20% DMSO compared with non-entrapped cells. The authors suggested that dehydrated PNIPAAm nanofibers may protect the entrapped cells by buffering them against the formation of large extracellular ice crystals.

Chen et al. developed a biomimetic fibrous scaffold, termed Cryosilk, to enhance cell manufacturing and cryopreservation (69). The scaffolds with core-shell structure were fabricated by integrating electrospinning, in situ surface functionalization, and freeze-shaping, comprising a fibroin/polyalanine (PAL) core and a sericin shell (Cryosilk@FAS). After slow freezing, the post-thaw viability of human MSCs (hMSCs) was significantly higher in Cryosilk@FAS (91.0%) compared to Cryosilk@FS (only fibroin fiber core and sericin shell) (77.5%). This improvement was attributed to enhanced measured thermal conductivity and inhibition of ice crystal growth. As a result, Cryosilk@FAS exhibited a faster thawing rate (128 °C/min) than Cryosilk@FS (75 °C/min), along with reduced temperature gradients and more uniform heat distribution. Furthermore, freeze-thawed BECs were shown to activate macrophage-mediated tissue repair in a murine excisional wound model.

An insightful study by Ran et al. explored scaffolds fabricated via electrospinning of silk fibroin/poly(ethylene oxide) blends and populated with bovine cartilage stem/progenitor cell pellets (70). Constructs were subjected to slow-cooling cryopreservation in a 10% DMSO/90% FBS mixture. The presented evidence indicates that thawed cells were able to effectively migrate from the pellets along the scaffold fibers, retaining growth and chondrogenic potential at levels comparable to

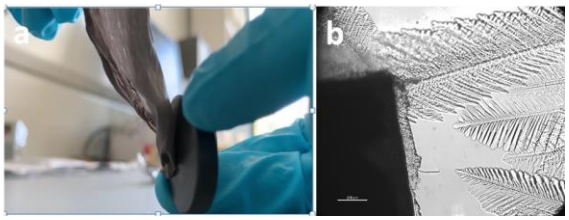

Figure 2. (a) Approaches for cryopreservation of electrospun nanofibrous scaffolds. Bulk PCL meshes supplemented with 5% $CoFe_2O_4$ nanoparticles, imparting magnetic properties and designed for vitrification and nanowarming; (b) Interaction of a PCL/PLA scaffold with an advancing ice front in a 5% DMSO solution during directional solidification on a cryostage (in collaboration with the Faculty of Agriculture, Food, and Environment, the Hebrew University of Jerusalem, Rehovot, Israel). Scale bar indicates 200 µm

fresh cells. Moreover, thawed cartilage equivalents were able to fully restore the trochlear defect in rats after 3 months of implantation.

As such, nanofibrous scaffolds exhibit high surface area, porosity, and elasticity, which inherently provide mechanical robustness that can help maintain scaffold integrity and support cell alignment and retention during cryopreservation. Rapanos et al. studied the effect of slow freezing on acellular electrospun mats composed of either PCL alone or a blend of PCL and chitosan (71). Cyclic tensile tests revealed that the freezing process (performed in phosphate-buffered saline without CPAs and with induced ice nucleation at –6 °C) did not significantly alter the mechanical properties of the fibers after 7 d of cryogenic storage. The authors attributed a slight increase in Young's modulus following freezing to altered crystallinity of the fibrous scaffolds. In line with this, Batnyam et al. investigated polyurethane as a scaffold material capable of retaining its elasticity at freezing temperatures (72). The research team demonstrated that slow freezing of mouse myoblast cells on electrospun polyurethane meshes, under protection of 10% DMSO, enhanced post-thaw cell recovery by minimizing cell detachment during freeze-thaw cycles.

The incorporation of diverse nanoparticles (NPs) into nanofibrous scaffolds has been widely studied in tissue engineering, particularly for applications in wound healing and skin regeneration (73, 74). In the context of cryopreservation, NPs have also gained increasing attention, especially in vitrification and advanced rewarming strategies such as laser photothermal heating (75) or nanowarming (76, 77), primarily for cell-laden hydrogel constructs.

Against this background, nanofibrous scaffolds can thus (i) be engineered to incorporate magnetic NPs either during fabrication ensuring homogeneous distribution within the fibers, or (ii) be exposed post-fabrication to NP-containing vitrification solutions. Recently, Leal-Marin et al. demonstrated the modification of electrospun scaffolds through the targeted integration of magnetic NPs (78, 79) for future cryopreservation applications (Fig. 2).

Beyond the conventional slow freezing and vitrification, directional freezing has emerged as a promising strategy for the cryopreservation of tissues, organs, and cell-biomaterial constructs (80). Using this approach, Mutsenko et al. demonstrated that HeLa cells cryopreserved on nanofibrous PCL/polylactic acid (PLA) scaffolds retained a substantial fraction of viable cells post-thaw (81).

In the 1980s, David Pegg explored the 'in-air' slow-freezing for rabbit cornea transplantation, which involved draining excess cryoprotectant prior to initiating cooling (82, 83). In our studies, the same approach enabled

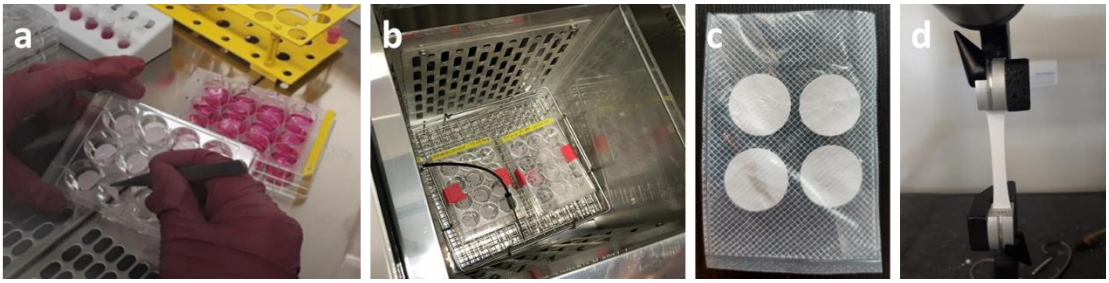

Figure 3. "In-air" cryopreservation workflow adapted for electrospun stem cell-seeded scaffolds: (a) cell seeding onto scaffolds; (b) in-plate cryopreservation; (c) cryopreservation in cryobags; (d) mechanical testing following cryopreservation.

the efficient cryopreservation of 3D cell-seeded collagen-hydroxyapatite (HA) constructs (58) and alginate core-shell macrospheres (84), highlighting its potential as a robust strategy for tissue engineering (Fig. 3). In line with this, Barker et al. extended the approach to PCL electrospun scaffolds seeded with SaOS-2 cells, employing cryobags (four BECs per bag) and using 10% DMSO or ethylene glycol (EG) as CPAs, with or without the addition of 0.3 M sucrose. This combination achieved ~80% post-thaw cell viability across all CPA formulations tested (85).

Currently, DMSO- and xeno-free approaches and CPA formulations are being explored for the cryopreservation of BECs (86, 87, 88). In line with this trend, we are conducting studies to evaluate GMP-compliant freezing solutions for the preservation of cell-seeded electrospun scaffolds (Fig. 4a and b).

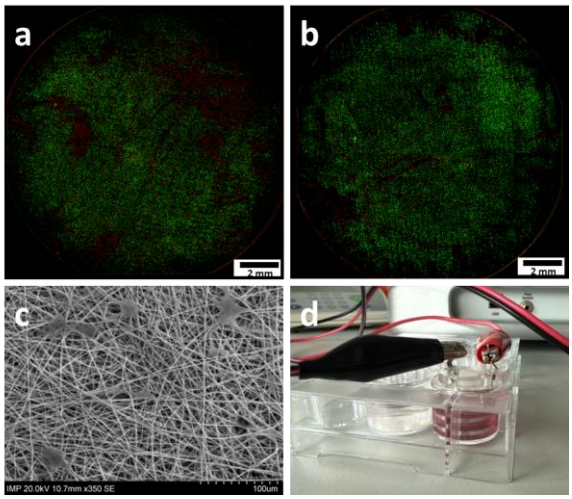

Figure 4. Fluorescent microscopy images of whole electrospun scaffolds seeded with SAOS-2 cells after "in air" freezing in cryobags in Stem-Cellbanker® DMSO-free (a) and Stem-Cellbanker® GMP (b) freezing solutions, respectively. Live-dead staining with Calcein-AM (live cells in green) and ethidium homodimer-1 (dead cells in red) on day 1 post-thaw. Up to 70% live cells were recovered in both cases. SEM picture of human bone marrow-derived (BM-MSCs) electroporated with 450 mM sucrose in suspension at 1500 kV/cm (8 pulses, 100 µs, 1 Hz,), frozen-thawed and then seeded on PCL/PLA electrospun scaffolds. Day 1 after reculture (c); Custom-designed electrode integrated with a BTX electroporation device for on-scaffold sugar delivery into cells for subsequent cryopreservation (d) (in collaboration with the University of Ljubljana, Faculty of Electrical Engineering, Ljubljana, Slovenia).

In the early 1980s, Igor Katkov introduced the use of electroporation into the field of cryobiology (89). This approach enabled electroporation-driven loading of stem cells with sugars as an alternative to DMSO-based cryopreservation of cell suspensions (90). The subsequent study expanded the range of sugars to include sucrose, trehalose, and raffinose for electroporation-assisted loading of umbilical cord-derived MSCs, paving the way for future tissue-engineering applications (91). Within DMSO- and xeno-free workflows, stem cells may (i) be electroporated in suspension and then cryopreserved for subsequent 3D construct colonization, or (ii) be electroporated and cryopreserved directly on the scaffold in a ready-to-use format after attachment (Fig. 4c and d). More recently, following this logic, electroporation conditions were adapted for the direct loading of cells attached to nanofibrous PCL/PLA electrospun scaffolds with sucrose, yielding a ready-to-use format for biopreservation (92).

Of equal importance, nanofibrous meshes fabricated by electrospinning hydrogel-forming polymers, either directly or through post-processing/functionalization with hydrogels, provide additional cryopreservation benefits, as demonstrated in the following several studies (93, 94). Interestingly, Xu et al. fabricated 3T3 cell-loaded, nanofibrous, degradable hydrogels based on hydrazone-cross-linked poly(oligo ethylene glycol methacrylate) using reactive electrospinning (93). The resulting constructs were immediately immersed in liquid nitrogen (LN_2) without any CPAs and stored frozen for 3 weeks. For recovery, the frozen scaffolds were thawed in preheated (37 °C) growth medium. Notably, the study reported sustained cell viability within the scaffolds, with 80% viability after one day and 87% after seven days compared to freshly prepared scaffolds. The proposed dual cryoprotective mechanism is thought to result from the macroscopic drying of the scaffold during electrospinning, which leaves minimal non-bound water to freeze, combined with the hydrogel nanofibers' ability to bind water, thereby inhibiting the formation of large ice crystals.

Exquisite biomimetic fibrous scaffolds fabricated by Chen et al. using electrospinning featuring a PLA/gelatin/graphene oxide core and an alginate-modified shell and termed CryoSiCo were used for cryopreservation of hMSCs (94).

Slow freezing with 10% DMSO and subsequent storage in LN_2 for 21 d were applied. The research group found that when hMSCs were cryopreserved within these scaffolds, high degree of post-thaw cell viability (92.8%) and proliferation were detected. The authors attributed these findings to the 3D culture environment, high thermal conductivity, and uniform heat transfer provided by the electrospun scaffolds, which protected the frozen cells from thermomechanical stress and cracking. Moreover, wound-healing studies in mice demonstrated therapeutic effects of freeze-thawed BECs on healing process, most likely due to the synergistic tissue-regeneration effects of both the scaffold and the hMSCs.

Likewise, nanofibrous elastic supports derived from natural materials [e.g., cellulose nanocomposites (95)] and fabricated by techniques other than electrospinning, such as melt blowing (96), can in turn can be integrated into more complex cryopreservation systems [e.g., cells entrapped into gelatin methacryloyl-collagen and frozen on melt electrowritten microfiber scaffolds (97)] offer an efficient framework for protecting a wide range of human cell types.

Notably, several studies exposed the challenges associated with freezing scaffold-free engineered cell sheets (98) or muscle equivalents (99) in the absence of elastic nanofibrous supports, leading to pronounced ECM disruption and associated changes in mechanical properties. Fibrous scaffolds can also be integrated into microfluidic chips to create hybrid platforms that combine drug discovery, tissue engineering, and on-chip cryopreservation capabilities. Özsoylu et al. functionalized a rigid sensor surface with elastic electrospun fibers as a cryoprotective support. This enabled on-biochip freezing and thawing of Chinese hamster ovary cells using 10% DMSO, significantly improving sensor performance compared to unmodified surfaces (100). Similarly, Kim et al. enhanced an organ-on-a-chip platform by incorporating electrospun PCL/Pluronic F108 membranes coated with ECM hydrogels (101). Even at 5% DMSO, post-thaw viability exceeded 90% across vascular, retinal, and blood-brain barrier models. Cellular functional markers remained robustly expressed during seven days of perfusion culture. Importantly, both the structural integrity and compositional properties of the electrospun membranes were well maintained after thawing.

ALGINATE ENCAPSULATION-MEDIATED CRYOPRESERVATION

The integration of hydrogel encapsulation into cryopreservation protocols represents a fundamental shift from a purely chemical approach to cryoprotection to one that leverages the principles of materials science, biophysics, and synthetic biology. Among the wide range of natural, synthetic, and supramolecular hydrogels, alginate remains the most widely used. This natural polysaccharide can be crosslinked by divalent cations to form stable hydrogels, a property that enabled the pioneering work of Lim and Sun in 1980, when they developed calcium alginate microcapsules for islet cell encapsulation (102). Current evidence demonstrates that alginate-based hydrogels are not merely inert scaffolds for holding cells; they function as active cryomodulatory matrices that create a controlled microenvironment, altering both the physical conditions (e.g., limiting ice crystallization and buffering osmotic and mechanical stresses) and strengthening cellular resilience required for successful cryopreservation (103). Conversely, the relatively large dimensions of alginate beads and capsules, combined with their high water content (>90%), low surface-to-volume ratio, and mechanically fragile semipermeable membrane, render these constructs particularly susceptible to cryodamage.

Here, we specifically outline distinct challenges associated with the cryopreservation of solid and coaxially fabricated, primarily alginate-based constructs, supplemented with a few examples from our own practice.

Cryopreservation of alginate-based cell-populated solid constructs

The ability of alginate encapsulation to protect such a sensitive to cryoinjury cell type as hepatocytes from the adverse effects of conventional cryopreservation by slow cooling was demonstrated in 1993 by Dixit et al. (104). Since that discovery, numerous studies have shown the feasibility of slow-cooling cryopreservation for different alginate encapsulated biological samples: human cultured and native as well as primary murine red blood cells (RBCs) (105), human (106), murine (107) and common marmoset monkey MSCs (108), human dermal fibroblasts (109), macrophages (110), recombinant C2C12 myoblasts (111, 112), human osteosarcoma MG63 cells (113),

isolated human primordial/primary follicles (114), HepG2 liver spheroids (115), rat hepatocytes (116), mouse testicular tissue (117), porcine cardiosphere derived cells (118) and rat neurospheres (119).

Moreover, integrating the expansion and cryopreservation of human embryonic stem cells whether as single cells, aggregates, or microcarrier-immobilized cells encapsulated in alginate resulted in high post-thaw recovery yields (>70%) (120). Crucially, alginate encapsulation combined with slow freezing in EG/trehalose supplemented with the ROCK inhibitorY-27632 yielded superior post-thaw outcomes (>80%) for induced pluripotent stem cells (iPSCs) compared with the standard DMSO/FBS (fetal bovine serum) freezing solution (121). This strategy was likewise highly effective for GES, U251, HepG2, A549, and 3T6 cell lines, achieving post-thaw viabilities exceeding 90%.

Umemura et al. employed a passive graded freezing protocol (4 °C for 5 min → −30 °C for 30 min → −80 °C for storage up to 28 d) to cryopreserve alginate-entrapped human dental pulp stem cells (122). Using an optimized gelation parameters and CPA cocktail consisting of 10% EG, 1.0 M sucrose, and 0.00075 M PVP, the cells retained high viability and proliferative capacity, as well as cell-surface antigen expression comparable to that of non-cryopreserved controls. Structural analyses further confirmed that the cryopreserved constructs remained intact and undamaged.

Several underlying mechanisms of the alginate encapsulation protective action during the cryopreservation have been revealed: ice crystal growth inhibition (117), osmotic buffering (123, 124), physical support and mechanical stress prevention (116). Moreover, alginate encapsulation reduces a cold-induced apoptosis (116), and increases the resistance to oxidative stress (125), important to support the post-warming recovery. Consequently, sodium alginate gel *per se* has been reported to be endowed with cryoprotective properties (126). In addition, encapsulation in non-adhesive alginates induces reversible cell cycle arrest (125, 127), resulting in increased stability of genetic information during the cryopreservation process.

The study by Ortiz Silva et al. demonstrated that alginate microspheres size notably affected cell survival after a slow cooling cryopreservation process, with a cell viability decline from 70% to 7% as the size increased from 200 to 2000 μm (110). Our previous studies demonstrated that cryopreservation outcomes can be improved by implementing controlled ice nucleation (106), resulting in nearly 90% cell survival within alginate spheres with diameters of 500-1000 μm.

According to Mohanty et al., the alginate concentration itself critically determines the cryopreservation response of encapsulated human dermal fibroblasts (109). When BECs prepared with 1.5-2% alginate were frozen in the absence of CPAs, their metabolic and angiogenic activities were preserved at levels comparable to those in CPA-supplemented groups (e.g., 5% DMSO or a combination of 5% glycerol, 5% PROH, and 200 mM trehalose). Conversely, the lower polymer and higher water fraction in 1% alginate matrices promoted maximal ice-driven pore size increase.

Another interesting aspect investigated by Naqvi et al. considers the effect of bone marrow stromal cell density (10×10^6 *vs.* 20×10^6 cells/ml) and pre-freeze cell priming in microcapsules on post-thaw recovery after slow-cooling cryopreservation with 10% DMSO (39). At higher cell density, the initial pre-freeze cell viability was lower and declined further after cryopreservation in both unprimed and primed samples. This trend was not evident in the unencapsulated samples.

Injectable alginate-gelatin microbeads were laden with hMSCs and subjected to slow cooling cryopreservation in 0.3 M trehalose and 10% DMSO (128). Although cryopreservation reduced the mechanical compressive strength and strain at failure and release of vascular endothelial growth factor (VEGF), post-thaw cell viability remained above 80% after 7 d in culture.

Apart from solid spherical beads, alginate encapsulation in the form of fibers provides higher surface area and improved mass transport, facilitating more uniform nutrient and cryoprotectant distribution. In this regard, Cao et al. compared rapid freezing of human RBCs in suspension with RBCs encapsulated in alginate microfibers. Under optimized conditions (fiber diameter ~720 μm and 2% sodium alginate), fiber-microencapsulation resulted not only in significantly higher RBC recovery but also permitted a reduction of glycerol concentration to 5% or less (129). In the slow freezing study by Cagol et al., human osteosarcoma MG63 cells encapsulated and cryopreserved in alginate

fibers, in particular when DMSO and glycerol were used as CPAs, showed larger metabolic activity and proliferative capacity compared to cells cryopreserved in suspension (113). In addition, alginate-water soluble chitin fibers designed by Lu et al. demonstrated an exceptional capacity for 3D slow cooling cryopreservation of human pluripotent stem cells in mFreSR® cryomedium (130).

The use of more complex cellular constructs for hydrogel encapsulation introduces additional challenges for cryopreservation. For example, alginate-encapsulated liver cell spheroids stored at −80 °C exhibited rapid and progressive deterioration in functional recovery after only a few weeks (131). In contrast, constructs stored at −170 °C maintained consistently high functional recovery over the course of a year. A multifaceted study by Lee et al. demonstrated that alginate beads generated after thawing porcine hepatocyte spheroids (frozen first and then encapsulated) showed greater potential as an "off-the-shelf" bioartificial liver system compared with the immobilized cryopreservation format, in which spheroids were encapsulated prior to freezing (50). The study further reported that cryopreservation in large-scale freezing bags and storage in LN_2 resulted in superior post-thaw construct performance relative to cryovial freezing and deep-freezer storage.

Chronologically, Kuleshova's Cryobiology Laboratory at the National University of Singapore achieved successful vitrification of a diverse array of scaffold-free and scaffold-based constructs (65, 132, 133, 134, 135). With respect to hydrogels, the group achieved exquisite post-vitrification functionality of hMSCs on microcarriers made from alginate coated with chitosan and collagen (136) and in alginate-fibrin beads (137) as well as of rat hepatocytes encapsulated in modified collagen (138, 139). In parallel, the Song's research group demonstrated effective vitrification of mouse insulinoma betaTC3 cells entrapped in calcium alginate/poly-L-lysine/alginate beads (140, 141). Subsequently, the use of hydrogel-based systems was expanded to the vitrification of pluripotent and multipotent stem cells (123), hMSCs (142, 143), 3D MSC spheroids (in gelatin methacryloyl) (144), recombinant C2C12 myoblasts (111), human umbilical vein endothelial cells (HUVECs) (145) and mouse preantral follicles (77).

Alginate microcapsules in combination with calcium ions promoted murine MSCs cryopreservation by vitrification at low total solute concentration of CPAs within 400 μm quartz microcapillaries when immersed into LN_2 given the sufficiently high cooling rate (146). Together with a small amount of Ca^{2+} supplementation, these factors were shown to be essential prerequisites for maintaining intact microcapsule morphology after rewarming and for significantly augmenting cell recovery.

In the elegant study by Wang et al., 5% (w/v) glycerol and 0.5 M trehalose were used as CPAs that were directly incorporated into the alginate-gelatin encapsulation mixture to produce capsules (diameter 1.0 ± 0.1 mm) (105). Encapsulated human RBCs were rapidly frozen in LN_2 and thawed in a 40 °C water bath. The authors achieved 75–80% post-thaw recovery while preserving excellent morphological and functional characteristics of both cultured and native human RBCs. In addition, cryopreserved murine RBCs showed circulation efficiency comparable to that of fresh RBCs in a mouse model. Of particular interest, compared to non-encapsulated group that exhibited peak cooling rates of 600–650 °C/min, the microcapsules achieved instantaneous peak rates of 15,000 °C/min.

In a related study, sheep RBCs were encapsulated within composite alginate microcapsules reinforced with cellulose nanocrystals (CNC) and subjected to both slow and rapid freezing in 0.5-0.9 M trehalose (147). Thawing was carried out in a water bath either at 37 °C or 25 °C for fast and slow thawing protocols, respectively. Consistent with this, the fast-freeze/fast-thaw strategy yielded RBC recovery rates exceeding 85% when 0.5 M trehalose was combined with a 2% CNC/1% alginate composite hydrogel. Several CNC-attributed underlying cryoprotective effects were elucidated, such as delayed ice formation, increased content of bound water, improved ice recrystallization inhibition, and superior protection against freeze-induced deformations.

Droplet-based vitrification of adherent human iPSCs on alginate microcarriers with reduced stiffness and a 4-h adhesion period resulted in a maximum recovered area of 42% (148).

For vitrification, the primary challenges are control of devitrification, CPA toxicity management, and enabling the cryopreservation of clinically relevant cell numbers. Hydrogel

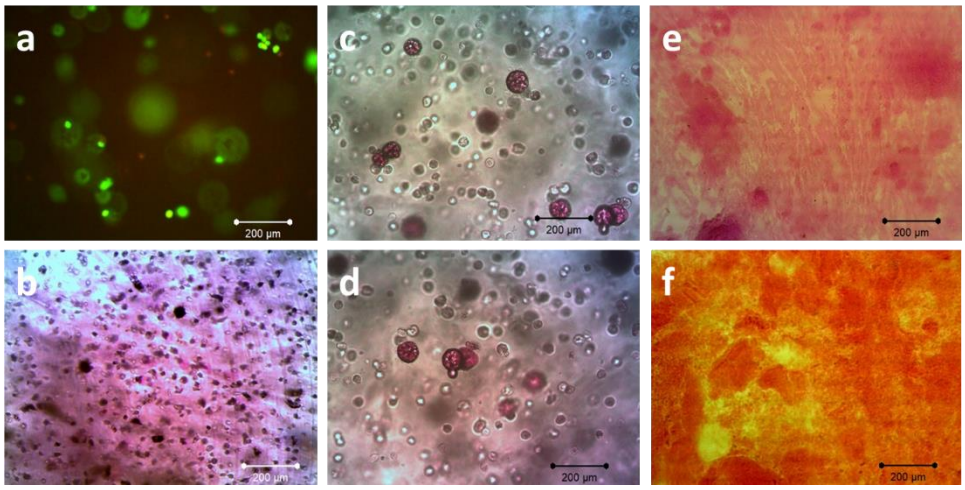

Figure 5. Effect of vitrification in DEPS-1 medium (10% DMSO, 20% EG, 20% 1,2-PD, 0.5 M sucrose) on MSCs encapsulated in alginate macrospheres. (a) FDA/EB staining showing live cells in green and dead cells in red; (b) MTT staining immediately post-vitrification, with dark purple formazan crystals indicating metabolically active cells; (c, d) Adipogenic differentiation before and after vitrification, visualized by Nile Red staining; (e, f) Osteogenic differentiation before and after vitrification, visualized by Alizarin Red staining.

encapsulation inhibits devitrification and the associated intracellular ice formation (IIF) during the cooling and warming stages (123). In general, the success of vitrification is a complex system where a change in one variable, such as the container type, solution composition, exposure, cooling and warming modes, sample type, necessitates an adjustment in others. We previously demonstrated that extending the total duration of the two-step exposure by 1 min and 45 s (from 1 min 15 s to 3 min) significantly increased the post-thaw viability of encapsulated MSCs by 70% (143). In follow-up work, we also confirmed that further prolongation of the two-step exposure to 4 min 30 s did not improve viability (remaining at 74%). Nonetheless, owing to the hydrogel dampening effect on CPA load, the less technologically demanding one-step exposure for 5 min achieved over 80% viability post-rewarming. As a result, MSCs vitrified within alginate hydrogel exhibited high viability and metabolic activity, as confirmed by Fluorescein Diacetate/Ethidium Bromide (FDA/EB) and methyl-thiazolyl-tetrazolium (MTT) staining, respectively, and retained their capacity for induced multilineage differentiation (142) (Fig. 5).

Cryopreservation of alginate-based cell-populated core-shell constructs

A distinct example of hydrogel encapsulation technology for tissue engineering applications is represented by core-shell multicompartmentalized 3D structures. As bioinspired scaffolds, these versatile platforms recreate specific cell niches for a range of purposes, including targeted cell and drug delivery, spheroid formation, *in vitro* disease modeling, and the secretion of bioactive factors, among others (149). However, compared with hydrogel constructs in which cells are entrapped within a bulk homogeneous gel network (e.g., solid micro- or macrospheres), core-shell structures present distinct cryopreservation challenges due to their unique architecture and physicochemical properties.

In our studies, core-shell capsules laden with MSCs were successfully frozen using an in-air approach (84). Our team used 10% DMSO combined with 300 mM sucrose as the CPA formulation, applying controlled slow cooling and an optimized CPA loading procedure. This protocol preserved both capsule integrity and post-thaw cell viability, consistent with the findings of Cui et al., who demonstrated that the structural integrity of >1 mm alginate capsules could be efficiently maintained by using the prioritized serum-free freeing media composed of 10% DMSO together with 300 mM glucose or trehalose (150). Their approach proved effective

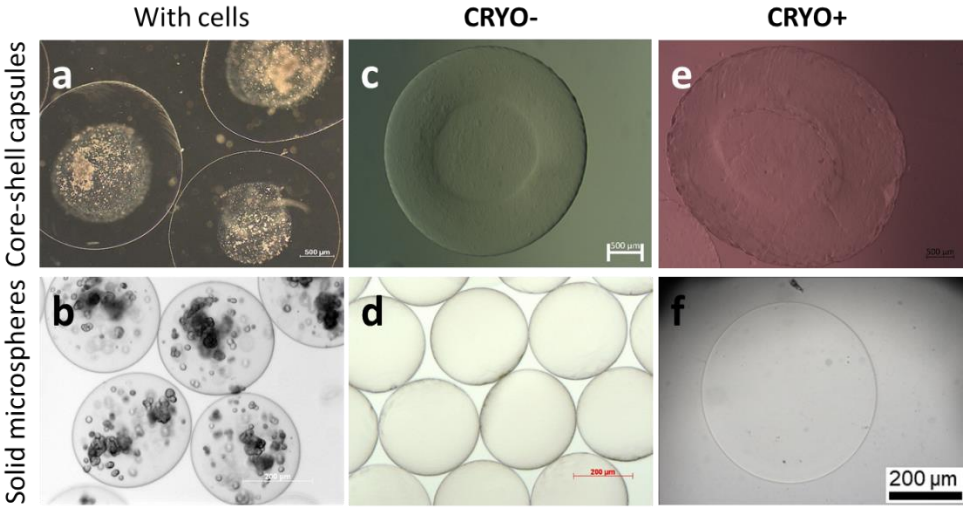

Figure 6. 3D alginate constructs fabricated from low-viscosity alginate using uniaxial (solid microspheres) and coaxial (core-shell capsules) electrospraying, applied as hydrogel-based cryopreservation systems. Upper panel: Cell-laden core-shell capsules (a) and acellular capsules prior to [(c), CRYO–] and after [(e), CRYO+] cryopreservation. Lower panel: Corresponding images for solid microspheres - (b) cell-laden, (d) acellular prior to cryopreservation, and (f) after cryopreservation. Cryopreservation procedure: Cell-free constructs were subjected to in-air slow freezing containing 10% DMSO and 300 mM sucrose following a 90-min CPA loading step and thawing at 37 °C for 30 s. Cell source: Amnion-derived MSCs from Callithrix jacchus. Scale bar: 500 µm (upper panel); 200 µm (lower panel).

across multiple mammalian cell types, including native retinal pigment epithelial (RPE) cells, genetically engineered RPE cells, HUVECs, and MSCs. In our accompanying study investigating the effects of cryoprotectant exposure time (45 and 90 min) and thawing temperature (37 °C and 60 °C) on the integrity of acellular core-shell capsules frozen in air (151), we observed that a higher proportion of intact capsules was achieved with longer incubation and higher thawing temperature. Specifically, an incubation time of 90 min combined with thawing at 60 °C resulted in approximately 70% intact capsules. The addition of 300 mM sucrose to 10% DMSO further improved capsule integrity. Nevertheless, it is worth noting that, due to the high water content of hydrogels, the in-air freezing approach may be less effective compared to other scaffold types.

Figure 6 displays a comparison of the general appearance of core-shell capsules and solid microspheres containing cells (Fig. 6A and B, respectively), as well as their corresponding acellular formats before (Fig. 6C and D) and after cryopreservation (Fig. 6E and F). As observed, unlike the isolated cells dispersed within the bulk hydrogel of solid beads, more complex cellular assemblies formed within the liquid core of the capsules. At the same time, the two-compartment configuration of capsules introduces distinct cryopreservation challenges related to uneven freezing dynamics.

Even during the equilibration stage with CPAs, the core-shell design demonstrates protective properties. In the study by Li et al., human hepatic stellate cells were encapsulated in alginate core-shell microcapsules (~230 µm in diameter) using a coaxial electrospray technique. The authors assessed the correlation between DMSO concentration (10-50% v/v), cell viability, and membrane blebbing (152). The semipermeable alginate shell buffered the diffusion of DMSO with reduced cellular bleb formation, and significantly improved cell viability compared to non-encapsulated cells. With core-shell alginate hydrogel microencapsulation, Qin et al. successfully achieved glycerol-free cryopreservation of human erythrocytes at a high final hematocrit (>40%) with high recovery (up to 95%) by using 500 mM trehalose as the sole cryoprotectant combined (153). It was further inferred that the

fabricated core-shell constructs exhibited enhanced heat transfer and protected the encapsulated cells from mechanical damage from the outside. In the study by Lu et al., the core-shell format was successfully extended to the cryopreservation of organoids (154). The authors encapsulated mouse gastrointestinal organoids in core-shell hydrogel capsules (OD ~1900 ± 25 μm and ID ~900 ± 40 μm) composed of a Matrigel™ core supporting organoid growth and an outer alginate shell produced by a two-fluidic electrostatic co-spraying method. For cryopreservation, the organoid-laden capsules were frozen under a slow-freezing protocol (controlled cooling at ~1 °C/min) in a medium containing 10% DMSO) and stored at –80 °C for six weeks before thawing. Post-thaw viability of organoids from capsules reached ~80%, substantially higher than the ~20% recovery from bulk Matrigel™ structure. The alginate shell was proposed to buffer mechanical and thermal stresses (such as ice/ice-crystal formation) during freezing and thawing, thereby improving organoid recovery. In the study by Tang et al. human umbilical cord MSCs were encapsulated within alginate-based core-shell microcapsules and cryopreserved in DMSO at concentrations ranging from 0% to 10% under slow freezing conditions (155). Following long-term storage and retrieval from LN_2, encapsulated cell viability showed no significant difference between the 5% and 10% DMSO groups, with both sustaining survival rates above 80%. It is noteworthy that even at a reduced DMSO concentration of 2.5%, post-thaw viability of MSCs remained above the 70% threshold considered clinically relevant. Furthermore, MSCs frozen-thawed in microcapsules retained their key functional attributes such as proliferation, surface markers expression, stemness and multi-lineage differentiation capacity. Interestingly, in the study by Pruß et al., the cryosurvival of sperm encapsulated in either solid beads or core-shell capsules was evaluated (156). Alginate-encapsulated sperm were cryopreserved in standard medium (i.e., INRA-82 extender supplemented with 2.5% (v/v) glycerol). Irrespective of the encapsulation mode, stallion sperm cryosurvival was significantly lower than that of conventionally diluted sperm; however, core-shell capsules markedly improved cold-storage outcomes compared to solid beads. In addition, the study revealed that calcium-induced alginate gelation significantly reduced sperm motility compared with barium, and that encapsulation in solid beads notably compromised sperm plasma membrane integrity. Storage of sperm in barium-alginate core-shell capsules did not affect sperm membrane integrity and motility during storage from 24 up to 96 h at 5 °C.

Even more noteworthy, the core-shell format (with an average diameter of approximately 2.2 mm) enabled the successful cryopreservation of high-hematocrit human RBCs using only 0.7 M trehalose for protection (157). With rapid cooling achieved by direct immersion into LN_2 on a stainless-steel grid, more than 85% of the alginate-encapsulated RBCs were recovered. After washing, the RBCs retained normal morphology and adenosine 5′-triphosphate levels and met established clinical transfusion criteria comparably to the commercial standard 17.5% hydroxyethyl starch.

Another rapid-cooling study demonstrated enhanced processing throughput enabled by the core-shell construct format combined with low CPA concentrations (158). The research team introduced a capillary microfluidic method to encapsulate porcine adipose-derived stem cells in alginate core-shell hydrogel microcapsules (~525 μm diameter, ~53 μm shell thickness) and cryopreserved them in a CPA solution composed of 1 M 1,2-propanediol (PROH) and 1 M EG, supplemented with trehalose/dextran. The cell-laden capsules were loaded into plastic straws and plunged into LN_2 for cooling, then rapidly rewarmed in a 37 °C water bath. Post-thaw viability consistently exceeded ~70% across all CPA formulations tested, and the surviving cells retained proliferation ability, expression of key surface markers, pluripotency-gene expression and multi-lineage differentiation capacity, comparable to that of fresh control cells. Despite the occurrence of recrystallization and devitrification during rewarming, the approach still enabled “ready-to-use” stem-cell/biomaterial constructs while substantially reducing CPA toxicity.

In addition to slow and rapid cooling, a series of studies on ice-free cryopreservation demonstrated that the core-shell design offers significant advantages, primarily by allowing the use of CPAs at far lower than typical concentrations, while also presenting certain technical challenges.

In the study by Song and Liu, the core-shell design enabled vitreous cryopreservation of large-volume (>500 μm) MSC-embedded

microcapsules with a low concentration (2 M) of penetrating CPAs (1 M PROH and 1 M EG supplemented with dextran and trehalose) (159). The constructs were fabricated using a microfluidic platform from sodium alginate and sodium carboxymethyl cellulose solutions. Following equilibration with the CPA solution, the capsules were loaded into conventional French straws and subsequently vitrified by direct submersion into LN_2. Cell viability and proliferation rates, expression of cell surface proteins, and induced differentiation ability were similar to the non-vitrified group. Nonetheless, statistically significant differences were observed in the expression of the stem cell gene Rex1 and proliferation marker Ki-67, which appeared to be affected by the cryopreservation procedure. Interestingly, Huang et al. developed a devitrification-inhibiting strategy based on core-shell alginate microencapsulation and optimization of CPAs for conventional plastic straws as well as quartz microcapillary for up to ~250 μL and up to ~2.5 μL sample volumes, respectively.

Using a cocktail of PROH and trehalose viability and functional properties of pluripotent and multipotent stem cells were well preserved (123). Absence of such protective microenvironments dramatically raised devitrification and IIF risk (a lethal event to cells) in non-encapsulated cells and caused irreversible damage to the microcapsules. In accordance with these findings, high post-rewarming cryosurvival of HUVECs (~80%) resulted from encapsulation in core-shell alginate microcapsules following low-CPA vitrification (up to 3 M of penetrating CPAs: 1.5 M EG, 1.5 PROH and 1 M trehalose) in the study by Li et al. (145). Furthermore, vitrified microencapsulated HUVECs preserved their original morphology and proliferative capacity comparable to fresh controls. It was also observed that larger capsules (~900 μm vs. ~400 μm) did not significantly impact post-vitrification cell survival, while enhancing encapsulation efficiency. Cryomicroscopy studies revealed plausible protective mechanisms, showing that microcapsules improved vitrification through the inhibition of ice crystals and devitrification. Cao et al. fabricated alginate constructs in a core-shell configuration with a diameter of 524 μm for large-volume (10 mL) vitrification of human umbilical cord blood-derived MSCs using a low concentration (~2.5 M) of penetrating CPAs (160). Successful outcomes (including intact microstructure, high cell viability, and excellent biological function) were achieved through this synergistic approach, which encompasses Fe_3O_4-nanoparticle-mediated nanowarming and a polytetrafluoroethylene capillary used as a flexible cryopreservation vessel. As a protective mechanism, the authors identified that in addition to inhibiting devitrification, the alginate hydrogel shell can mitigate overheating of the cells enclosed in the core by physically separating them from nanoparticles in the solution outside the constructs.

Low-CPA vitrification (0.75 M EG, 0.75 M PROH, 1 M trehalose and 10% (w/v) dextran T50) in a core-shell format was successfully extended beyond capsules to microfibers in the study by Tian et al. (161). Here, umbilical cord-derived MSCs were encapsulated into continuous alginate microfibers (core diameter ~200 μm, shell thickness ~150 μm) fabricated via coaxial microfluidics and vitrified using a custom nylon-mesh loading device. Encapsulated hMSCs displayed post-thaw viability above 80%, retained attachment and proliferation efficiency, maintained normal morphology, and preserved surface marker expression and differentiation capacity comparable to the fresh control group. Consistent with the above cryomicroscopy observations, the results from this research group confirmed that alginate hydrogel can suppress ice formation and growth during both the cooling and rewarming phases.

CRYOPRESERVATION OF BULK 3D MICRO- AND MACROPOROUS CELL-POPULATED SCAFFOLDS

Cryopreserving macroporous bulk scaffolds is particularly demanding because their intricate pore architecture and ECM-cell interactions are highly sensitive to thermal and osmotic stresses. Consequently, maintaining the scaffold's structural integrity, particularly pore interconnectivity, and mechanical properties is critical, as any compromise can undermine cell survival, function, and post-implantation tissue integration.

This section addresses a heterogeneous category of biomimetic, cell-populated scaffolds, including cryogels, spongy matrices, carriers, and microspheres. Most of these systems are characterized by highly porous architecture,

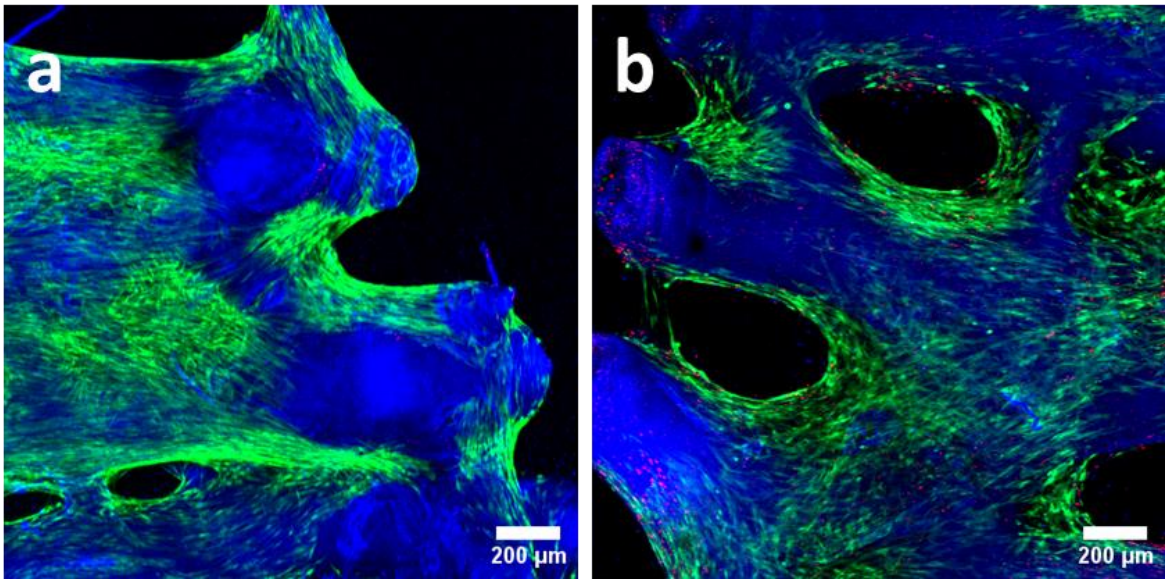

Figure 7. Cryopreservation of model 3D macroporous scaffolds derived from the chitin sponge *Ianthella basta* and seeded with h MSCs. Constructs were cultured for 14 d and cryopreserved by slow cooling in 10% DMSO. Cryopreserved constructs exhibited a significantly higher propensity for cell death, primarily at the periphery (b), compared with non-frozen controls (a). Live and dead cells were stained with FDA (green) and EB (red), respectively, while blue fluorescence indicates he chitin matrix stained with Calcofluor White (in collaboration with the Institute of Experimental Physics, TU Bergakademie Freiberg).

often with interconnected pores. Such an architecture not only facilitates cell adhesion and nutrient diffusion but also enables the even distribution of CPAs throughout the scaffold interior.

The feasibility of using slow cooling for 3D porous BEC preservation has been demonstrated in several earlier reports (162, 163, 164). A primary determinant of success is preserving the scaffold's structural integrity. In this regard, Teo and colleagues revealed freezing-induced deformations in the scaffold microstructure, with more pronounced deformations in denser ECM (165). Interestingly, Liu et al. observed that vitrified porous HA scaffolds (1 cm in diameter and 2 cm long) fractured more easily than scaffolds frozen by the two-step method (163). The authors also reported that higher-density HA scaffolds exhibit greater resistance to cryopreservation-induced damage than lower-density scaffolds. From a mass-transport perspective, bulk 3D scaffolds typically require longer exposure times to achieve homogeneous CPA permeation and distribution (166). Using Optimaix™ porous collagen hMSC-populated scaffolds (6 mm diameter x 1.5 mm thick), Petrenko et al. demonstrated that perfusion bioreactor-based slow-cooling cryopreservation offers clear benefits over diffusion-driven methods by facilitating more efficient CPA delivery and removal (167). Also, in vitrification, the bioreactor was used for stepwise introduction and elution of vitrification solutions through the thickness of the constructs (168). Equivalent amounts of viable cells were recovered when orbital shaker (treatment in discrete steps) and bioreactor (gradual treatment) were used for cell treatment.

Even under identical freezing conditions, different biocompatible biomaterials can exhibit varying responses to the thermal stresses of cryopreservation. In a study illustrating this, Chinnasami et al. evaluated HA and poly(l-lactic acid) (PLLA) cell-free scaffolds subjected to cooling rates of 1, 10, and 40 °C/min down to −75 °C, followed by 24 h storage in LN_2 and thawing at 37 °C (169). Simple macroscopic observations demonstrated that ceramic scaffolds disintegrated completely at slower cooling rates (1 and 10 °C/min) and partially at 40 °C/min. In contrast, PLLA scaffolds retained their structure under all conditions, highlighting the superior thermal resilience of this thermoplastic polymer.

In line with this, Ren et al. have recently established a comprehensive platform

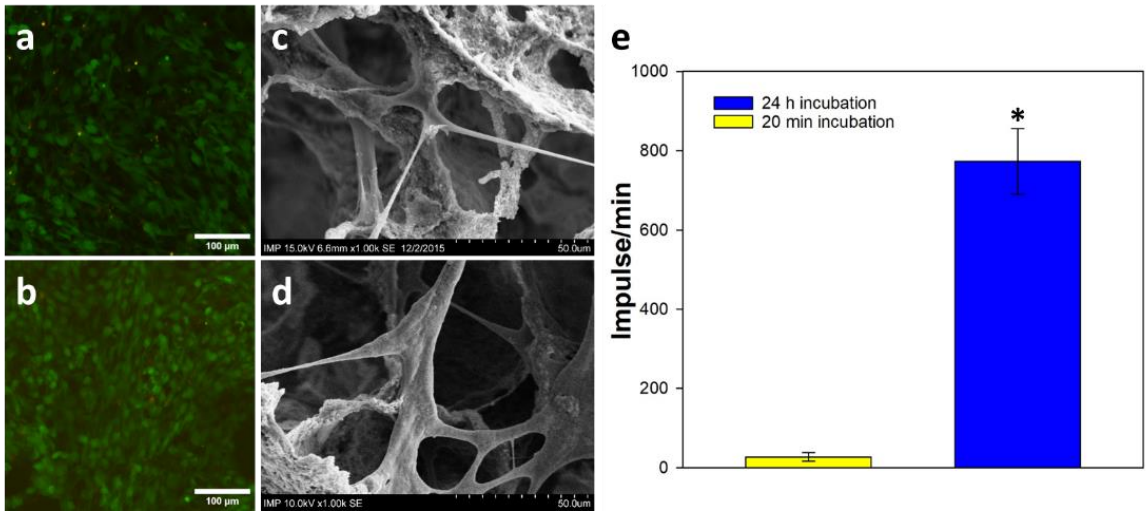

Figure 8. Laser scanning microscopy images of non-frozen control constructs (a) and constructs subjected to in-air freezing in 10% DMSO and 300 mM sucrose following overnight preincubation in 100 mM sucrose (b). Cell viability was assessed by Calcein AM and EthD-1 staining (green = live cells; red = dead cells). SEM images of the control (c) and frozen-thawed (d) constructs illustrate cell attachment and spreading within macroporous collagen-HA scaffolds (in collaboration with the Centre for Translational Bone, Joint and Soft Tissue Research, Faculty of Medicine of Technische Universität Dresden). Uptake of [^{14}C]sucrose by human dermal MSCs (e). A total of 1 × 10^5 cells were cultured in growth medium supplemented with [^{14}C]sucrose (2.5 mCi/mmol; Amersham) for either 20 min (control) or 24 h. Following incubation, cells were harvested, washed three times with PBS, and radioactivity was measured using an SL-40 liquid scintillation counter (Intertechnique, France). * - denotes statistically significant differences between groups ($p < 0.05$, Student's t-test).

integrating cryopreservation, thawing, and transplantation based on 3D poly(D,L-lactic acid) (PDLLA) porous microspheres (PMs), a biomimetic matrix hydrogel (BMH), neural stem cells (NSCs), and human umbilical cord mesenchymal stem cell-derived exosomes for spinal cord injury repair (2). A standard freezing medium composed of 10% DMSO and 20% FBS was used for slow-cooling cryopreservation experiments. Compared to free NSC spheroids, the viable cell ratio in NSC@PM constructs was significantly higher. The authors attributed this result to the "anchorage" provided by the PMs, which was considered crucial for maintaining cell viability during the freeze–thaw process of the composite constructs. PDLLA PMs are characterized by a uniform spherical morphology (average diameter of 270.7 ± 47.7 µm) and interconnected pores with an average size of 26.1 ± 5.8 µm.

Beyond structural considerations, the intrinsic vulnerability of adherent cells within BECs to cryoinjury has been documented in several reports, with post-thaw viability often limited to around 50% (162, 164, 170). However, these initial experimental attempts documented the critical importance of tissue engineering parameters (for example, cell type, confluency and scaffold internal architecture or coatings) for cryopreservation success.

Culture conditions prior to cryopreservation may also influence post-thaw cell survival. Accordingly, Miyoshi et al. reported that ~65% of initially seeded fibroblasts remained attached to porous scaffolds (2 × 2 × 2 mm^3) made of polyvinyl formal resin after thawing when cells were pre-cultured for 24 h prior to cryopreservation (40). This study also highlighted collagen coating of scaffolds as a promising strategy to further increase fibroblast immobilization efficiency and consequently improve cell growth after thawing. Later, Katsen-Globa et al. found that a 2-h pre-cultivation period was optimal for the cryopreservation of hMSCs in alginate-gelatin cryogels (171). This duration provides a balance between adequate cell-matrix adhesion and a flexible cytoskeleton that can withstand thawing-induced mechanical stress. Shorter pre-culture (0.5 h) left cells insufficiently anchored, resulting in significant loss after thawing, whereas prolonged culture (24 h) reduced viability, likely due to excessive cytoskeletal stabilization and stronger adhesion forces that

make cells more vulnerable to mechanical damage during cryopreservation.

Cell density is another key parameter in tissue engineering and cryopreservation. In this regard, Liu et al. found that higher pre-freeze osteoblast densities on HA scaffold surfaces enhanced post-thaw attachment and viability, suggesting a beneficial role of cell-cell interactions (172). Conversely, Matsumura et al. reported that beyond an optimal threshold, increasing pre-freeze cell density adversely affects post-thaw relative integrity of human fibroblasts within collagen sponges (20 mm in diameter and 1 mm in thickness) (173). This effect underscores intercellular mechanical stress and membrane deformation, often referred to as the "packing effect," which is ultimately responsible for increased cell injury.

A two-layered spongy matrix composed of hyaluronic acid and atelocollagen was developed as a scaffold for the cryopreservation of human skin fibroblasts (164). The resulting BECs (4 cm × 3 cm) were frozen in a polystyrene dish at a rate of −1 °C/min from 4 °C to −60 °C, followed by transfer to storage temperatures of either −152 °C or −85 °C. BECs cryopreserved in 10% DMSO/20% FBS at −85 °C for 6 months or at −152 °C for 1 year retained cell viability, proliferative capacity, and VEGF secretion, comparable to the control sample stored at −152 °C for 3 weeks, which had 56.2% viability immediately post-thaw.

Consistent with above observations, our own results demonstrated that the viability of hMSCs cryopreserved on chitin scaffolds (Fig. 7) was reduced by about 30% compared to the same cells cryopreserved in suspension (174), highlighting the challenges associated with maintaining cell survival in large spongy systems during freezing and thawing.

Tissue-engineered human bone grafts investigated in a study by Tam et al. were composed of decellularized bovine bone disks (8 mm in diameter and 5 mm in height) and seeded with human iPSC-derived mesenchymal progenitor cells (175). They were subjected to slow freezing using a commercially available cryomedium containing 10% DMSO and storing at –80 °C. Following cryopreservation, the authors observed structural alterations of the ECM at both the edges and the center of the grafts. These changes were accompanied by a significant decline in cellular metabolic activity, a reduced number of viable cells, and an increased presence of cleaved caspase-3, particularly after 24 h of post-thaw recultivation. These studies demonstrates that several factors are essential determinants of post-thaw viability, including cell type, cell state, and scaffold material properties (e.g., stiffness, porosity), which greatly impact cell adhesion.

Several later slow freezing studies have been reported to improve cryopreservation outcomes. For example, "in-air" freezing and cell pretreatment with sucrose (58) had a positive effect on the viability (Fig. 8a and b) and functional activity (Fig. 8c and d) of amnion-derived MSCs from common marmoset monkey within 3D bulk collagen-HA scaffolds. Similarly, Rogulska et al. and Trufanova et al. demonstrated a synergistic improvement in post-thaw recovery of hMSCs in 3D hydrogels and macroporous collagen matrices, respectively, following overnight pre-incubation with 100 mM sucrose and freezing in its presence (42, 176). In addition to its well-known roles in promoting cell dehydration, reducing the propensity for intracellular ice formation and stabilizing cellular membranes, sucrose may also confer direct intracellular protection, as suggested by our follow-up [^{14}C]sucrose incorporation studies (Fig. 8e). This finding is particularly noteworthy, as substrate-attached cells are especially prone to intracellular ice formation [via paracellular ice penetration (177, 178)] and thus susceptible to the associated cryoinjury during cryopreservation.

Yang et al. cryopreserved rat BM-MSC-laden 3D β-TCP scaffolds (~78% porosity) using 10% DMSO/20% FBS and stepwise cooling (4 °C → −20 °C → −70 °C → LN_2) (179). Cell survival rate was reported to be 81.3% and alkaline phosphatase activity was unaffected by cryopreservation. More complex types of constructs, consisting of 3D-bioprinted osteoblastic structures (12 mm in diameter and 1 mm in height) and β-TCP scaffolds (11 mm in diameter and 2 mm in height) infiltrated with osteoblasts encapsulated in a gelatin-alginate hydrogel, were cryopreserved by Hernández-Tapia et al. (180). The constructs were subjected to in-plate slow cooling in the presence of 20% DMSO. The study demonstrated that immature osteoblasts required a longer recovery period than mature osteoblasts, and that a longer pre-cryopreservation culture period (7 d *vs.* 3 d) had a beneficial effect on the post-thaw maintenance of metabolic activity and construct function, particularly when β-TCP scaffolds were used. However, even under optimal conditions,

approximately 14 d of post-thaw culture were required for the constructs to regain metabolic activity levels comparable to non-frozen controls. Similarly, Leppik et al. observed that hMSCs on β-TCP scaffolds (ChronOS Granules, 1.4-2.8 mm), frozen in air with 10% DMSO and 25% human serum, regained about 40% of their metabolic activity within the first two days post-thaw (181). The study further indicated that these cells were able to regain activity levels comparable to control non-frozen cells only at the later time points. Notably, all examined osteogenic genes showed higher expression in the frozen group compared to the non-frozen cells. Macroporous gelatin-based microcarriers (CultiSpher-S beads with a diameter of 130-380 µm) were cellularized either with goat BM-MSCs or mouse osteoblastic cell line MC3T3-E1 and cultured for a total of 1 week before cryopreservation (170). Different DMSO-based freezing media were assessed while the constructs underwent slow cooling to –80 °C at –1.5 °C/min and were subsequently transferred to LN_2 for 1 week.

A general tendency for shorter mean recovery time was observed for MSCs than for MC3T3-based constructs for the same CPA used 10% DMSO. A more recent study by Simitzi and colleagues demonstrated the feasibility of cryopreserving human skeletal muscle-derived cells on poly(lactic-co-glycolic acid) microcarriers (mean diameter ~300 µm) (182). Cellularized microcarriers were subjected to controlled slow freezing in the clinically approved DMSO-based solution CryoStor10. BECs showed cell viability ≥74% immediately after rapid thawing and ≥62% at 24 h post-thaw. Notably, neither the physico-mechanical characteristics of the microcarriers nor the cells' ability to differentiate into myotubes was compromised.

Carboxymethyl cellulose cryogel scaffolds (5 mm in diameter and 2 mm in thickness) were seeded with murine AML12 cells and subjected to slow freezing in 5% DMSO and 20% FBS (183). The scaffolds promoted spheroid self-assembly, facilitated faster diffusion and removal of the cryoprotectant compared to cell suspensions, and preserved both structural integrity and cellular metabolic activity at levels comparable to control samples. Gelatin cryogels (8 mm × 2 mm) fabricated via cryogelation were used to cryopreserve HepG2 and HUVEC cells (184). BECs were saturated with a DMSO-based cryomedium, incubated at 4 °C for 10 min, and stored directly in plates at −80 °C. Plates were then thawed at 37 °C in an incubator. Cells were frozen for 1 d or 1 month and subsequently recovered in culture for 1, 4, or 7 d. For both cell types, viability and proliferation were generally unaffected across all storage durations and recovery periods, except for HUVECs after 1-d cryopreservation followed by 1-d recovery, which showed a significant decrease compared with non-cryopreserved control.

Despite these encouraging attempts, studies exploring strategies to improve the efficiency of cryopreserving bulk 3D cell-seeded scaffolds constitute only the early phase of establishing an optimal protocol. The challenge of preserving these constructs can hardly be overcome without methods that prevent ice crystallization.

Vitrification, which avoids ice formation by solidifying the system into a glass-like state, offers a compelling alternative (6). Using this cryopreservation approach, osteoblasts seeded

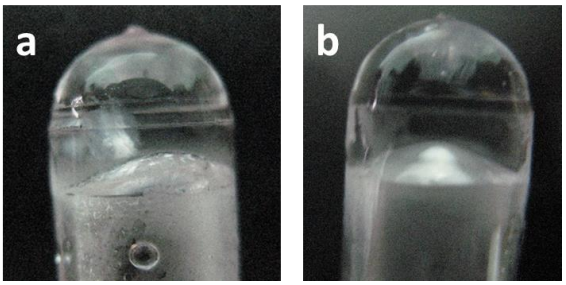

Figure 9. Porous alginate-gelatin scaffolds during the warming stage following rapid cooling in vitrification solutions. (a) DEPS 15/20/20 (15% DMSO, 20% EG, 20% 1,2-PD, 0.5 M sucrose), showing crystallization indicated by whitening in the scaffold center; (b) DEPS 15/20/20 supplemented with 1% PVA, showing no visible crystallization (scaffold remains transparent).

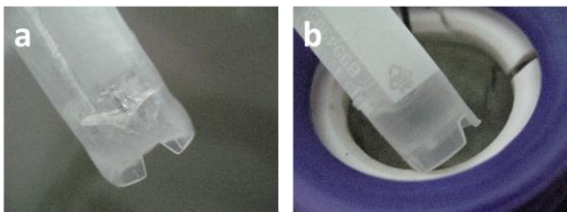

Figure 10. Effect of cooling regimen on cracking of vitrified alginate-gelatin scaffolds. (a) Cracking observed after direct plunging into LN2; (b) Stable glassy state achieved by two-step cooling with gradual temperature changes through the glass transition region.

on HA scaffolds and protected with 40% DMSO, 40% glycerol, or the vitrification solution VS55 exhibited post-thaw viabilities of 78%, 79%, and 83%, respectively (163). The study by Yin et al. used vitreous solution named as VS442 containing 40% DMSO, 40% EuroCollins solution and 20% basic culture medium. Likewise, vitrification maintained high cell viability, proliferative capacity, and osteogenic differentiation of osteoinduced canine bone marrow MSCs in partially demineralized bone matrices (185). Moreover, the study by Kang and Bae features successful vitreous cryopreservation MCF-7 cancer cell line in porous poly(lactic-co-glycolic acid) microspheres with no noticeable difference in cell viability, metabolic activity and resistance to doxorubicin (47). In a notable study by Zhi Wang *et al.*, tenocyte-scaffold constructs were fabricated on three types of polydimethylsiloxane surfaces - smooth, micro-grooved, and porous - and subjected to a multi-step vitrification protocol. Upon rewarming, constructs with a porous surface exhibited the highest number of viable tenocytes compared to the remaining scaffold types. This finding univocally indicates that a porous scaffold surface, as a key element of the cellular microniche, strongly promotes cell adhesion and survival rate (~93% *vs.* ~76% pre- and post-vitrification, accordingly) during cryopreservation (186). In another study, Dahl et al. reported exceptional post-vitrification outcomes for 1-mm-thick tissue-engineered blood vessels constructed from polyglycolic acid mesh seeded with porcine smooth muscle cells (187). Although apoptosis rates and mechanical strength were comparable to those observed with slow freezing, the metabolic activity of cells was significantly higher following ice-free preservation. Polymer cylindrical scaffolds (10 mm in diameter and ~1.9 mm thick) with 90% porosity were seeded with articular chondrocytes, cultured, and induced to chondrogenesis in a bioreactor for 7 d (168). The VS70 solution (3.97 M DMSO, 3.97 M Formamide and 2.83 M PROH) formulation introduced to constructs on an orbital shaker resulted in 56% chondrocyte viability level observed post-vitrification.

Despite their promising outcomes, the aforementioned studies reveal several challenges encountered by the ice-free approach. The principal hurdle lies in the high concentration of CPAs required to attain an amorphous state. Prior to the initiation of cooling, the viscous CPA cocktail must entirely saturate a bulk porous scaffold with a filigree interconnected geometry. The potential cytotoxicity of the vitrification solution imposes additional challenges on cells within a 3D scaffold. Furthermore, scaffold regions that are insufficiently permeated with CPA are less likely to achieve a stable glassy state, resulting in the formation of detrimental ice crystals. In case of BECs, fracture of vitrified solutions has been demonstrated to be detrimental to attached cells (43). The study demonstrated that solution fracturing and de-vitrification caused ~20% and ~17% cell damage, respectively, in cells attached to cylinder-shaped HA constructs during vitrification.

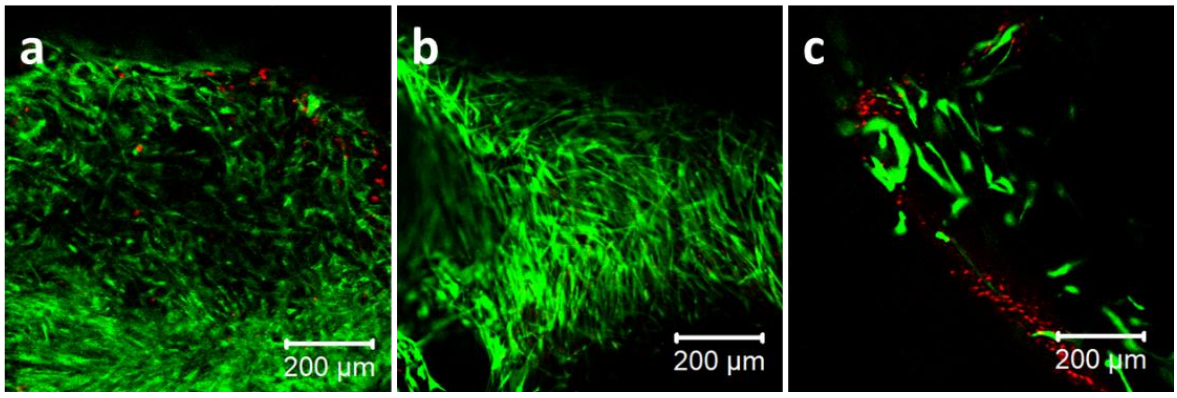

Figure 11. Laser scanning microscopy images showing the distribution and viability of MSCs within alginate-gelatin porous scaffolds: (a) control, (b) after exposure to DEPS 15/20/20 solution supplemented with 1% PVA, and (c) after vitrification. Cell viability was assessed using FDA/EB staining (live cells shown in green and dead cells in red, respectively).

In this regard, one of us have also demonstrated (188) that the heterogeneous porous structure of alginate-gelatin scaffolds (5 mm in diameter and 1 mm in thickness) promoted ice crystallization during the rewarming phase (Fig. 9a). This challenge was effectively circumvented by adjusting the composition of the vitrification cocktail, for example, through the addition of 1% polyvinyl alcohol (PVA), a synthetic ice blocker (Fig. 9b).

Vitrification demands ultra-rapid cooling and warming rates to "outrun" the ice formation. Achieving these rates uniformly throughout a relatively large 3D construct is extremely difficult. The surface of the scaffold may cool quickly enough, but the core will inevitably lag behind, creating a thermal gradient that allows for ice crystallization. Another important challenge the vitrification of BECs faces is a thermo-mechanical stress and a cracking of formed glass, which can be prevented by a slow temperature changes under the temperature region near the glass transition temperature (Tg) to provide enough time for relaxation of thermo-mechanical stresses (188, 189). Thus, cooling by immediate plunging into LN_2 results in notable cracking, damaging scaffold (Fig. 10a), while the two-step cooling (a plunging into LN_2 for 25 s, then keeping over the nitrogen mirror until the system solidified) completely avoids cracking (Fig. 10b).

Vitrification solutions can be toxic to cells due to the high concentrations of CPAs they contain, and cryobiologists are actively working on developing less toxic solutions and protocols including organs and BECs (190, 191). One of us showed that solution toxicity can be controlled by optimization of its composition and the exposure procedure time so that the cell viability after the exposure of a 3D porous scaffold to a solution of cryoprotectants is similar to the control (Fig. 11 a and b). Vitrification of 3D constructs faces a formidable obstacle: while a given protocol may yield high viability for cells in suspension (188), the same protocol often results in a catastrophic loss of viability when cells are seeded within a macroporous scaffold (Fig. 11c).

Of note, even when the bulk extracellular CPA solution is successfully vitrified, the physical interface between the cell membrane and the scaffold material appears to act as a potent catalyst for the formation of lethal ice crystals within the cell. While contact-mediated nucleation may remain negligible for cells in suspension, it becomes the primary cause of damage for cells within a 3D construct. Consistent with this, while vitrification solution VS55 has been reported to support nearly 85% osteoblast recovery after vitrification (43), it caused a marked decline in cell viability and osteogenic potential when applied to MSC-based 3D constructs (185).

Overall, the successful cryopreservation of large microporous cell-laden 3D scaffolds remains a significant challenge. Either way, the observed disparities in 3D porous BEC cryopreservation either using freezing or ice-free approaches point to a few crucial cryobiological phenomena: contact-induced intracellular ice nucleation, the inherent propensity of adherent cells for intercellular ice propagation via cell-cell and cell-matrix interactions (178, 192), their vulnerability to high concentrations of potentially toxic CPAs and cryopreservation-induced delayed onset cell death. Consequently, future research should prioritize strategies to specifically inhibit contact-induced intracellular ice formation, develop and deploy less toxic CPAs and ice-blocking compounds, customize every step of the cryopreservation protocol, and enhance cellular resistance to cryoinjury.

RECORDING OF FREEZING PATTERNS IN BECS

In BECs, the absence of vitrification and devitrification is typically assessed by simple visual inspection, distinguishing opaque, ice-crystallized regions from a transparent glassy state (43, 111, 145, 188). To overcome the limitations of this qualitative approach, more advanced techniques are employed, including cryomacroscope systems (193), an optical fiber (194) and microcomputed tomography (195), differential scanning calorimetry, differential thermal analysis, and X-ray diffraction (196).

Even though invasive, thermocouples are commonly employed to verify and calculate critical cooling and thawing rates in vitrification studies, with type T copper-constantan thermocouples being the most frequently used (197, 198). In the context of nanowarming, thermocouples present specific challenges, such as interference with radiofrequency fields, which can be mitigated through the use of alternative fine-gauge thermocouples (199). In freezing studies, thermocouples are commonly used to detect the onset of ice formation, perform heat-

transfer analyses (153), as well as quantify cooling and rewarming rates in BECs (200). This enables confirmation of artificially induced ice nucleation (106), including high-subzero freezing protocols, or verification of its absence in supercooling preservation techniques (201).

Thermocouples generally provide high accuracy for localized temperature measurements within biological tissues when inserted into cryovials or freezing bags. Moreover, for bulk BECs, constructs with complex geometries, or in cases where multiple BECs are frozen simultaneously, the number of thermocouples must be increased to adequately capture the full thermal history. The embedding of thermocouples into biological tissues (especially thin and delicate engineered tissues) as foreign material can compromise their structural integrity. Furthermore, the presence of multiple probes may further disturb the local thermal environment, potentially altering freezing dynamics and even promoting premature ice nucleation (202). Thermocouples have been routinely used in a number of studies on BEC cryopreservation to measure cooling and warming rates, as well as to confirm nucleation events (65, 153, 203). Thermocouples are often radially centered in "dummy" cryocontainers containing only the freezing medium (111, 204), or in construct-containing systems with either a single thermocouple (105, 205) or multiple thermocouples (43, 69). In sterile settings, direct insertion of thermocouples into the sample is often avoided due to contamination risks, and alternative placements (e.g., surrogate containers or external locations) are used, potentially compromising measurement accuracy.

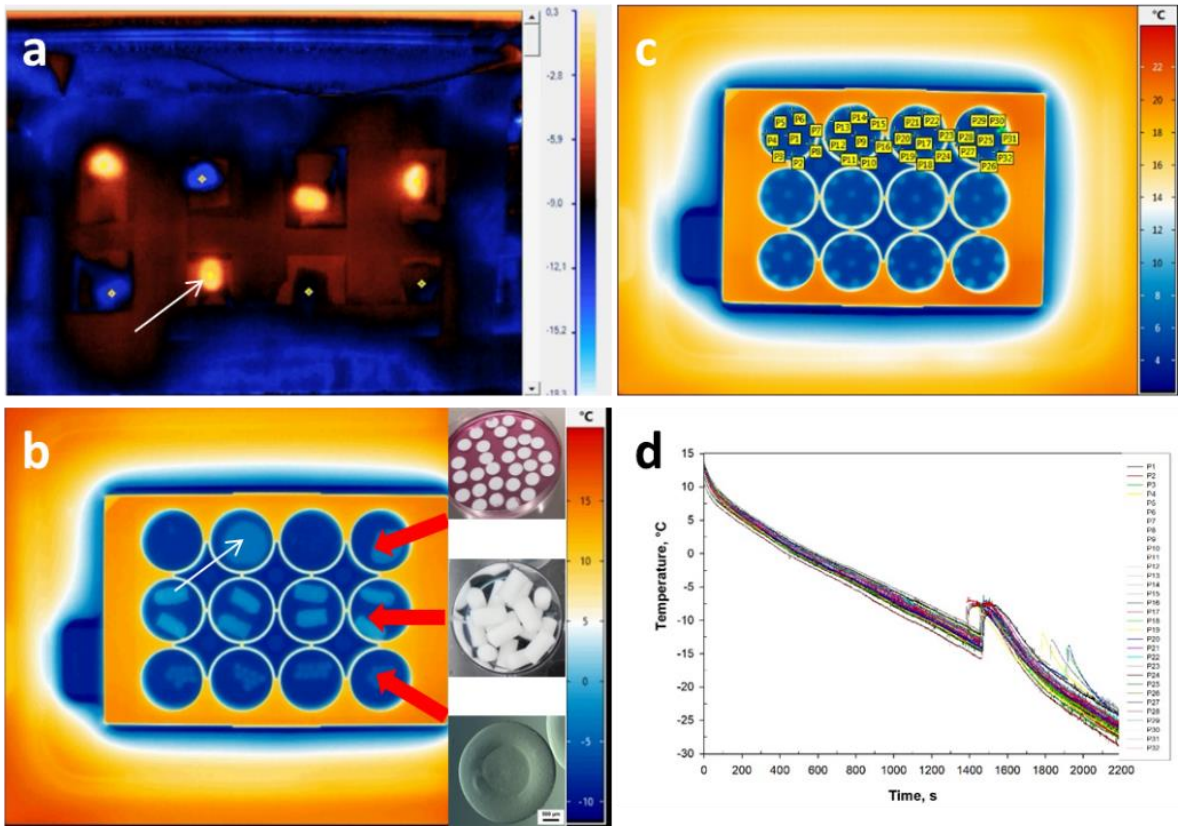

Figure 12. IRT facilitates the monitoring of freezing patterns in various BECs and freezing conditions. (a) Differential image of collagen-HA scaffolds frozen in cryobags; the white arrow indicates latent heat release by a frozen scaffold; (b) Infrared image of a culture plate containing different BECs: electrospun PCL/PLL scaffolds (top row), collagen-HA scaffolds (middle row), and core-shell alginate macrospheres (bottom row). The white arrow highlights latent heat release in the electrospun scaffold, while the red arrows and figure insets present macroscopic views of the corresponding accelular scaffolds; (c) Simultaneous pointwise analysis of freezing profiles of alginate core-shell macrocapsules positioned in the top raw and (d) The respective freezing curves derived from individual capsules (in collaboration with the Institute of Forming Technology and Forming Machines, Leibniz University Hannover (LUH, Garbsen).

The ability to measure thermal responses in BECs on a contactless basis offers cryobiologists a valuable complementary tool for optimizing cryopreservation. Beyond its traditional uses, infrared thermography (IRT) has emerged as a powerful, non-invasive technique, particularly advancing research in cryobiology-related fields such as *in planta* cryopreservation, cryosurgery, freeze-drying and temperature-controlled cryoprinting (206, 207, 208, 209, 210).

Compared to thermocouples, which provide point-based temperature readings at specific locations, several studies have demonstrated that IRT can effectively record the thermal profiles of plant material and mammalian cells in multiwell plates undergoing cryopreservation screening (211, 212, 213). It enables precise mapping of thermal gradients and ice front dynamics, real-time non-invasive monitoring of construct behavior during freeze-thaw procedures, and a deeper understanding of localized cryoinjury risk zones within BECs. Furthermore, in the BEC cryopreservation workflow, infrared thermography was employed to track the laser-induced and magnetic-induction heating responses of nanoparticles embedded in the vitrification solution or within nanocomposite hydrogels (77, 214).

Our more recent work has compared IRT with thermocouple readouts to observe freezing dynamics in porous collagen-HA scaffolds (215). The technique enabled contactless tracking of crystallization events, supercooling, and nucleation behavior under different cryoprotective conditions (215). Figure 12 offers a concise overview of how IRT has been applied to monitor freezing events in various BECs, based on our cryobiology practice.

In a model hydrogel system mimicking a blood vessel, IRT showed promise for extrapolating temperatures at specific intragel depths, supporting its use in monitoring freeze-thaw dynamics in hydrogel BECs (208).

It must be noted that, although IRT does not involve physical intrusion, it is typically limited to surface temperature measurements, whereas thermocouples can capture intraconstruct temperatures. Combining both methods can yield a more comprehensive thermal profile during BEC cryopreservation, which is essential for developing optimized preservation strategies in tissue engineering. An example is provided by the study of Reiterdank et al., in which thermocouples and infrared imaging were combined during supercooling to monitor the thermal history of vascularized composite allografts in real time, with the aim of optimizing preservation efficacy (201).

REGULATORY CONSIDERATIONS FOR TRANSLATING CRYOPRESERVATION OF BECS TO CLINICAL APPLICATIONS

Looking toward clinical implementation, the bench-to-bedside translation of BECs requires systematic progression through preclinical and clinical stages, alongside regulatory evaluation (216). The establishment of BEC banks at hospitals remains a crucial manufacturing constraint for their transition from laboratory development to clinical application and commercialization (217). Fabrication and especially cryopreservation of BECs has advanced in the past decade; however, translating laboratory findings into a clinical setting has been challenging because guidelines of Current Good Manufacturing Practice (cGMP) are often ignored in an academic setting.

Numerous publications refer to clinical trials/animal studies using BECs, but they do not address considerations for cryopreservation (49, 218, 219). A cGMP facility is the basis of any production for clinical application since any cell product must be produced under the regulations of 21 CFR (Code of Federal Regulations) Parts 1270 and 1271. In addition, Měřička et al. described that to use any tissue/product of human origin, the European Union's regulation of cell and tissue procurement, processing, storage and distribution and the directive of the European Parliament and Council (2004/23/EC) and European Commission directives (2006/17/EC and 2006/86/EC) have to be taken into consideration (220). The first hurdle that must be overcome is the use of United States Pharmacopeial Convention (USP)/GMP grade chemicals to produce the BEC and that adds significant costs and, in some cases, can cause different results due to fewer impurities than research grade. In addition, the robustness of the supply chain for materials must be guaranteed so that no or minimal disruption occurs. Furthermore, the right choice of CPA is crucial in combination with incubation time/temperature and cooling rate (221, 222). On that note, during GMP manufacturing all timelines are extended since the process follows a batch record and involves extensive sampling.

The extended contact times with a CPA such as DMSO can be challenging for the functionality and integrity of the BEC. The FDA allows an injection of a cell product with up to 10% DMSO. Such exposure may be associated with adverse effects that depend on infusion volume and patient health status (223). The maximum recommended DMSO dose is 1 g/kg body weight, although typical cell therapy infusions and BEC applications are generally well below this threshold. Nevertheless, developing cryopreservation recovery protocols suitable for GMP manufacturing (e.g., effective DMSO removal from a BEC prior to patient exposure) represents a key step in the translational pathway and is receiving wide experimental attention in cryobiological research (224). In parallel, the development of DMSO-free or DMSO-sparing CPAs remains an important complementary objective of ongoing cryobiological efforts (225).

In addition, the contact time of the respective CPA must be validated for the duration of the fill and finish with assuming the worst-case scenario (226). An underrated factor is the available devices to cool the BEC during loading/fill and finish (221). In cGMP ice is generally prohibited so alternatives are cold packs or blocks. Another unavoidable fact is that for freezing BECs only CoolCells or Controlled-Rate Freezers (CRFs, with or without LN_2 usage) are available, and the preferred method and freezing equipment also need to be validated for the produced BEC. An additional critical consideration is the logistical framework for storing, processing, and shipping BECs within clinically appropriate packaging (such as bags and vials) (222) and storage systems that adhere to established quality and regulatory standards (221, 227). Additionally, to cryopreserve the final product, the starting material must be chosen carefully. As an example, iPSCs have gained significant importance in tissue engineering and 3D cryopreservation (228). Especially allogeneic iPSCs-derived cell therapies are now the preferred platform for manufacturing of BECs. In a recent review, the challenges and differences between EU and USA have been reported (229). After manufacturing, the BEC needs to be stored and when the patient is available, shipped to the clinical site to be transplanted. This is a point of variability since breaches in the cold chain (customs, delays in shipping, and many more) have a significant impact on cell recovery, engraftment and function (230).

In general, thawing of BEC in the clinic is restricted due to clinical Standard Operating Procedures (SOPs), which can be hard to change. The current SOP is to thaw the patients BEC in a water bath at 37 °C but this could be adapted to water free thawing devices (PlasmaTherm, VIA Thaw, ThawStar CB). New organ preservation research uses nanoparticles and radio frequency (231) or other means of rapidly warming the BECs or organs (232), but the translatability of the approach must be evaluated by the Food and Drug Administration (FDA)/European Medicines Agency (EMA) (221, 227, 233) to make sure that they comply with 21 CFR Parts 1270 and 1271 and cGMP regulations and does not endanger the patient. Another important aspect that should be considered is the ethical issue and conflict of interest which has been summarized by Lu et al. and is not discussed here (234).

With the rapid advancement of bioprinted constructs toward clinical application (235, 236), their cryopreservation in accordance with GMP regulations is becoming essential for their safe storage and shipment from the production site to the patient.

Sustained interdisciplinary collaboration between cryobiology and medical community, engineers, and regulatory experts is essential to standardize biofabrication and preservation methods, including vitrification protocols tailored for 3D constructs (237).

CONCLUSION

Collectively, the remarkable co-evolution of cryopreservation and tissue engineering underscores sustained multidisciplinary efforts focused on preserving engineered living systems. As reviewed here, this endeavour has created integrated platforms and practical solutions, making the cryopreservation of cell-populated BECs both technically feasible and scientifically validated.

In particular, the robust mechanical resilience of elastic nanofiber mats enable attached cells to withstand the cryopreservation-related stresses. In turn, hydrogel-based constructs take advantage of their hydrated polymer networks to stabilize encapsulated cells, organoids, and microtissues throughout cooling and rewarming. In contrast, the cryopreservation

of 3D bulk micro- and macroporous cell-populated scaffolds remains considerably more challenging. Their complex pore architectures and variable diffusion and transport characteristics make it difficult to control ice formation, to achieve stable amorous state, and ensure consistent cell survival post-cryopreservation.

The incorporation of advanced thermographic imaging to noninvasively monitor freezing dynamics across BECs of varying geometries demonstrated by us here offers a remote straightforward means to strengthen quality-control frameworks.

Thus, the concept of *in toto* cryopreservation of fully assembled BECs to extend their lifespan marks a significant step forward in tissue engineering and is particularly appealing; however, in practice, the clinical reach of cryopreserved BECs requires the integration of multiple biomaterial- and cell-specific protective strategies, as well as harmonized quality control measures.

Acknowledgements: The authors thank Dr. Victor P Grischuk from the Institute for Problems of Cryobiology and Cryomedicine (IPC&C) for his valuable technical support in performing the ^{14}C-sucrose incorporation studies. This study was partially supported by National Research Foundation of Ukraine (project number 2021.01/0276).

Our research groups' long-term collaborative efforts, specifically the multidisciplinary partnerships between the IPC&C, National Academy of Sciences of Ukraine and the Institute for Multiphase Processes, LUH as well as those between LUH and University of Thessaly have primarily focused on the cryopreservation of macroporous scaffolds or cryogels, electrospun nanofibrous mats, and stem cells encapsulated in alginate. Accordingly, this review primarily highlights these and related construct types, drawing on examples from our own original cryobiological research.

REFERENCES

1. Langer R & Vacanti JP (1993) *Science* **260(5110)**, 920-926.
2. Ren J, Li J, Wang H, Feng H, Hao H, Chen J et al. (2026) *Bioactive Materials* **60**, 401-424.
3. Budharaju H, Sundaramurthi D & Sethuraman S (2024) *Biofabrication* **16(4)**, 042008.
4. Ziani K, Saenz-del-Burgo L & Pedraz JL, Ciriza J (2025) *International Journal of Molecular Sciences* **26(14)**, 6908.
5. Arutyunyan I, Elchaninov A, Sukhikh G & Fatkhudinov T (2022) *Stem Cell Reviews and Reports* **18(4),** 1234-1252.
6. Kuleshova LL, Gouk SS & Hutmacher DW (2007) *Biomaterials* **28(9),** 1585-1596.
7. Neves LS, Rodrigues MT, Reis RL & Gomes ME (2016) *Expert Review of Precision Medicine and Drug Development* **1(1)**, 93-108.
8. Rogulska OY, Trufanova NA, Petrenko YA, Repin NV, Grischuk VP, Ashukina NO, et al. (2022) *Journal of Biomedical Materials Research Part B, Applied Biomaterials* **110(2),** 489-99.
9. Acker JP, Bondarovych M, Brunotte R, Buriak IA, Fuller BJ, Glasmacher B, et al. (2020) in *Cell Engineering and Regeneration*, (eds) Gimble JM, Marolt Presen D, Oreffo ROC, Wolbank S & Redl H, Springer International Publishing, Cham, pp 1-69.
10. Spurrier RG, Speer AL, Grant CN, Levin DE & Grikscheit TC (2014) *The Journal of Surgical Research* **190(2),** 399-406.
11. Gorti GK, Lo J, Falsafi S, Kosek J, Quan SY, Khuu DT, et al. (2003) *Archives of Otolaryngology - Head & Neck Surgery* **129(8)**, 889-893.
12. Lyu S-R, Kuo Y-C, Ku H-F & Hsieh W-H. (2013) *Colloids and Surfaces B: Biointerfaces* **103**, 304-309.
13. Lavoie A, Fugère C, Beauparlant A, Goyer B, Larouche D, Paquet C, et al. (2013) *Tissue Engineering Part A* **19(7-8),** 1023-1038.
14. Grant L, Raman R, Cvetkovic C, Ferrall-Fairbanks MC, Pagan-Diaz GJ, Hadley P, et al. (2019) *Tissue Engineering Part A* **25(13-14)**, 1023-36.
15. Töpfer E, Pasotti A, Telopoulou A, Italiani P, Boraschi D, Ewart M-A, et al. (2019) *Toxicology in Vitro* **61,** 104606.
16. Lee BE, Lee BJ, Lee KJ, Lee M, Lim YJ, Choi JK, et al. (2022) *Biochemical and Biophysical Research Communications* **595**, 14-21.
17. Bissoyi A, Tomás RMF, Gao Y, Guo Q & Gibson MI (2023) *ACS Applied Materials & Interfaces* **15(2),** 2630-8.

18. Park JJ, Lee OH, Park JE & Cho J (2024) *Biopreserv Biobank*. **22(5),** 486-96.
19. Ohkawara H, Miyagawa S, Fukushima S, Yajima S, Saito A, Nagashima H, et al. (2018) *BMC Biotechnology* **18(1),** 56.
20. Shajib MS, Futrega K, Franco RAG, McKenna E, Guillesser B, Klein TJ, et al. (2023) *Journal of Tissue Engineering* **14**, 20417314231176901.
21. Ogawa T, Kajiya M, Horikoshi S, Yoshii H, Yoshino M, Motoike S, et al. (2022) *Regen Therapy* **20,** 117-125.
22. Kasai Y, Morino T, Dobashi I, Mori E, Yamamoto K & Kojima H (2021) *Frontiers in Bioengineering and Biotechnology* **9**, 687946.
23. Pitstick AL, Poling HM, Sundaram N, Lewis PL, Kechele DO, Sanchez JG, et al. (2022) *Stem Cell Reports* **17(8)**, 1889-1902.
24. Wiersma LE, Avramut MC, Lievers E, Rabelink TJ & van den Berg CW (2022) *Stem Cell Res Ther.* **13(1)**, 208.
25. Arai K, Murata D, Takao S, Verissiomo AR & Nakayama K (2020) *PLOS ONE*. **15(4),** e0230428.
26. Rawal S, Harrington S, Williams SJ, Ramachandran K & Stehno-Bittel L (2017) *Cryobiology* **76**, 41-50.
27. Nakayama-Iwatsuki K, Yamanaka T, Negishi J, Teshima J, Tamada Y, Hirabayashi M, et al. (2020) *Islets* **12(6)**, 145-155.
28. Shimizu T, Akahane M, Ueha T, Kido A, Omokawa S, Kobata Y, et al. (2013) *Cryobiology* **66(3)**, 326-332.
29. Oktay K, Marin L, Bedoschi G, Pacheco F, Sugishita Y, Kawahara T, et al. (2022) *Fertility and Sterility* **117(1),** 181-192.
30. Yamanaka T, Nakayama-Iwatsuki K, Fujimoto S, Hirono N, Negishi J, Tamada Y, et al. (2021) *Transplantation Proceedings* **53(5),** 1744-1750.
31. Kong Q, Stavrev D, Rahimi G, Todorov P, Pei C, Isachenko E, et al. (2026) *Journal of Ovarian Research* **19(1),** 55.
32. Eslahi N, Hadjighassem MR, Joghataei MT, Mirzapour T, Bakhtiyari M, Shakeri M, et al. (2013) *International Journal of Nanomedicine* **8**, 4563-4576.
33. Miyoshi H, Ohshima N & Sato C (2013) *Journal of Tissue Engineering and Regenerative Medicine* **7(1)**, 32-38.
34. Liu G, Shu C, Cui L, Liu W & Cao Y (2008) *Cryobiology* **56(3),** 209-215.
35. Vishwakarma SK, Lakkireddy C, Bardia A, Paspala SAB & Khan AA (2019) *Materials Science and Engineering: C* **102**, 34-44.
36. Herrmann FEM, Lamm P, Wellmann P, Milz S, Hagl C & Juchem G (2019) *Biomaterials* **212**, 87-97.
37. Rodríguez-Martínez D, Martínez-Losa MM & Alvarez-Dolado M (2017) *PLoS One* **12(1),** e0170776.
38. Magalhães R, Nugraha B, Pervaiz S, Yu H & Kuleshova LL (2012) *Biomaterials* **33(3)**, 829-836.
39. Naqvi SM, Gansau J & Buckley CT (2018) *Biomedical Materials* **13(3),** 034106.
40. Miyoshi H, Ehashi T, Ohshima N & Jagawa A (2010) *Artificial Organs* **34(7),** 609-614.
41. Seddighi MR, Griffon DJ, Schaeffer DJ, Fadl-Alla BA & Eurell JA (2008) *Veterinary Journal (London)* **178(2),** 244-250.
42. Trufanova N, Rogulska O, Semenchenko O, Mishchenko O (2025) *Problems of Cryobiology and Cryomedicine* **35(2)**, 103–109.
43. Liu BL & McGrath J (2024) *Cell Preservation Technology* **2(2)**, 133-143.
44. Jeong Y-M, Bang C, Park M, Shin S, Yun S, Kim CM, et al. (2021) *Cells* **10(3)**, 589.
45. Chen R, Wang B, Liu Y, Lin R, He J & Li D (2018) *Cryobiology* **82**, 1-7.
46. Kim JJ, Hebisch M, Kwak SS, Zheng M, Nuli S, Bae J-S, et al. (2025) *Scientific Reports* **15(1),** 12543.
47. Kang SW & Bae YH (2009) *Biomaterials* **30(25),** 4227-4232.
48. Cummins KA, Crampton AL & Wood DK (2019) *Tissue Eng Part C Methods* **25(1),** 25-36.
49. Fitzpatrick E, Filippi C, Jagadisan B, Shivapatham D, Anand H, Lyne M, et al. (2023) *PLoS One* **18(7)**, e0288185.
50. Lee J-H, Park H-J, Kim Y-A, Lee D-H, Noh J-K, Jung J-G, et al. (2024) *Scientific Reports* **14(1),** 12168.
51. Jitraruch S, Dhawan A, Hughes RD, Filippi C, Lehec SC, Glover L, et al. (2017) *Cell Transplant.* **26(8),** 1341-1354.
52. Altmaier S, Meiser I, Lemesre E, Chanrion B, Steeg R, Leonte LE, et al. (2022) *Reproductive Toxicology* **111,** 68-80.
53. Kilbride P, Lamb S, Gibbons S, Bundy J, Erro E, Selden C, et al. (2017) *PLoS One* **12(8)**, e0183385.
54. Brookshaw T, Fuller B, Erro E, Islam T, Chandel S, Zotova E, et al. (2024) *Cryobiology* **117**, 105155.

55. Mei J, Sgroi A, Mai G, Baertschiger R, Gonelle-Gispert C, Serre-Beinier V, et al. (2009) *Cell Transplant*. **18(1),** 101-110.
56. Aoki T, Koizumi T, Kobayashi Y, Yasuda D, Izumida Y, Jin Z, et al. (2005) *Cell Transplant.* **14(9),** 609-620.
57. Selden C, Bundy J, Erro E, Puschmann E, Miller M, Kahn D, et al. (2017) *Scientific Reports* **7(1),** 14518.
58. Mutsenko V, Knaack S, Lauterboeck L, Tarusin D, Sydykov B, Cabiscol R, et al. (2020) *Cryobiology* **92,** 215-230.
59. Fahy GM & Wowk B (2021) *Methods Mol Biol*. **2180**, 27-97.
60. Kay A & Kuleshova L (2016) in *Low Temperature Materials and Mechanisms*, (ed.) Bar-Cohen Y, CRC Press, Boca Raton, pp 349-394.
61. Wowk B (2010) *Cryobiology* **60(1),** 11-22.
62. Campbell LH & Brockbank KGM (2022) *Cells* **11(7)**, 1115.
63. Owida HA, Al-Nabulsi JI, Alnaimat F, Al-Ayyad M, Turab NM, Al Sharah A, et al. (2022) *Applied Bionics and Biomechanics* **2022,** 1953861.
64. Suamte L & Babu PJ (2024) *Nano TransMed.* **2024,** 100055.
65. Wen F, Magalhães R, Gouk SS, Gajadhar B, Lee KH, Hutmacher DW, et al. (2009) *Tissue Engineering Part C: Methods* **15(1)**, 105-114.
66. Costa PF, Dias AF, Reis RL & Gomes ME (2012) *Tissue Engineering Part C: Methods* **18(11),** 852-858.
67. Bissoyi A, Pramanik K, Panda NN & Sarangi SK (2014) *Cryobiology* **68(3)**, 332-342.
68. Maeda T, Kim Y-J, Aoyagi T & Ebara M (2017) *Fibers* **5(1)**, 13.
69. Chen J, Xu Y & Ning X (2022) *International Journal of Biological Macromolecules* **221**, 723-735.
70. Ran J, Fei Y, Wang C, Ruan D, Hu Y, Zheng Z, et al. (2021) *ACS Biomaterials Science & Engineering* **7(3),** 881-892.
71. Repanas A, Lauterboeck L, Mavrilas D & Glasmacher B (2016) *Scholars Academic Journal of Biosciences* **4(10),** 818-821.
72. Batnyam O, Suye S-I & Fujita S (2017) *RSC Advances* 7(81), 51264-51271.
73. Palani N, Vijayakumar P, Monisha P, Ayyadurai S & Rajadesingu S (2024) *Journal of Nanobiotechnology* **22(1)**, 211.
74. Dang Z, Ma X, Yang Z, Wen X & Zhao P (2024) *Polymers* **16(1)**, 24.
75. Chang T, Moses OA, Tian C, Wang H, Song L & Zhao G (2021) *Advanced Science* **8(6),** 2003387.
76. Liu X, Zhao G, Chen Z, Panhwar F & He X (2018) *ACS Applied Materials & Interfaces* **10(19),** 16822-35.
77. Tian C, Shen L, Gong C, Cao Y, Shi Q & Zhao G (2022) *Nature Communications* **13(1)**, 7515.
78. Leal-Marin S, Höltje K, Lopera A, Garcia C, Glasmacher B & Gryshkov O (2022) *Problems of Cryobiology and Cryomedicine* **32(4),** 303 (abstract).
79. Leal-Marin S, Gallaway G, Höltje K, Lopera-Sepulveda A, Glasmacher B & Gryshkov O (2021) *Current Directions in Biomedical Engineering* **7(2),** 460-463.
80. Arav A & Natan Y (2024) *Regenerative Medicine Reports* **1(2)**, 137-148.
81. Mutsenko V, Chasnitsky M, Sirotinskaya V, Müller M, Glasmacher B, Braslavsky I & Gryshkov O (2021) in *8th European Medical and Biological Engineering Conference 2020*, (eds) Jarm T, Cvetkoska A, Mahnič-Kalamiza S & Miklavcic D, Springer International Publishing, Cham., pp 391-398.
82. Fong LP, Hunt CJ & Pegg DE (1987) *Current Eye Research* **6(4),** 569-577.
83. Fong LP, Hunt CJ, Taylor MJ & Pegg DE (1986) *The British Journal of Ophthalmology* **70(10),** 751-760.
84. Gryshkov O, Mutsenko V, Tarusin D, Khayyat D, Naujok O, Riabchenko E, et al. (2021) *International Journal of Molecular Sciences* **22(6),** 3096.
85. Barker S-A, Glasmacher B & Gryshkov O (2021) in *SPhERe – Proceedings of the 4th International Symposium on Pharmaceutical Engineering Research –S,* 15 - 17 September 2021, Braunschweig, https://doi.org/10.24355/dbbs.084-202110251042-0.
86. Ng JY, Tan KYF & Ee PLR (2022) *Biomacromolecules* **23(7)**, 2803-13.
87. Wang J, Shi X, Xiong M, Tan W-S & Cai H (2022) *Cryobiology* **104,** 47-55.
88. Zhou S, Zhang K, Li M, Qi K, Jia D, Guan F, et al. (2025) *Adv. Healthcare Mater.* **14(4),** e2404228.
89. Katkov I (2002) *Problems of Cryobiology* **2002(2)**, 3-8.
90. Dovgan B, Barlič A, Knežević M & Miklavčič D (2017) *The Journal of Membrane Biology* **250(1),** 1-9.

91. Mutsenko V, Barlič A, Pezić T, Dermol-Černe J, Dovgan B, Sydykov B, et al. (2019) *Cryobiology* **91**, 104-114.
92. Gryshkov O, Mutsenko V, Dermol-Černe J, Miklavčič D & Glasmacher B (2021) in *8th European Medical and Biological Engineering Conference* 2020, (eds) Jarm T, Cvetkoska A, Mahnič-Kalamiza S & Miklavcic D, Springer International Publishing, Cham, pp 485–494.
93. Xu F, Dodd M, Sheardown H & Hoare T (2018) *Biomacromolecules* **19(11)**, 4182-4192.
94. Chen J, Zhao Y, Zhou A, Zhang Y, Xu Y & Ning X (2022) *International Journal of Biological Macromolecules* **211**, 159-169.
95. Anton-Sales I, Roig-Sanchez S, Sánchez-Guisado MJ, Laromaine A & Roig A (2020) *ACS Biomaterials Science & Engineering* **6(9),** 4893-4902.
96. Abe K, Nakamura-Yamada S, Hayashi I, Hirashima K, Nishimura F, Katagiri W, et al. (2026) *Journal of Oral and Maxillofacial Surgery, Medicine, and Pathology* **38(3)**, 396-404.
97. Janssen J, Chirico N, Ainsworth MJ, Cedillo-Servin G, Viola M, Dokter I, et al. (2024) *Biomater Sci.* **12(15),** 3866-81.
98. Freitas-Ribeiro S, Carvalho AF, Rodrigues DB, Martins L, Pires RA, Mendes VM, et al. (2025) *Bioactive Materials* **46,** 301-310.
99. Gapinske L, Clark L, Caro-Rivera LM & Bashir R (2023) *Tissue Engineering Part A* **29(21-22),** 557-568.
100. Özsoylu D, Isık T, Demir MM, Schöning MJ & Wagner T (2021) *Biosensors and Bioelectronics* **177**, 112983.
101. Kim D, Yi S, Park B-u, Lee SJ, Lee J, Kim DS, et al. (2025) *ACS Macro Letters* **14(5)**, 622-629.
102. Lim F & Sun AM (1980) *Science* **210(4472)**, 908-910.
103. Benson EE, Harding K, Ryan M, Petrenko A, Petrenko Y & Fuller B (2018) *CryoLetters* **39(1),** 14-38.
104. Dixit V, Darvasi R, Arthur M, Lewin K & Gitnick G (1993) *Transplantation* **55(3),** 616-622.
105. Wang E, Liu S, Wang X, Zhang B, Ma D, Gao L, et al. (2025) *Chemical Engineering Journal* **516,** 163979.
106. Pravdyuk AI, Petrenko YA, Fuller BJ & Petrenko AY (2013) *Cryobiology* **66(3)**, 215-222.
107. Gurruchaga H, Ciriza J, Saenz Del Burgo L, Rodriguez-Madoz JR, Santos E, Prosper F, et al. (2015) *International Journal of Pharmaceutics* **485(1-2)**, 15-24.
108. Gryshkov O, Hofmann N, Lauterboeck L, Pogozhykh D, Mueller T & Glasmacher B (2015) *Cryobiology* **71(1),** 103-111.
109. Mohanty S, Wu Y, Chakraborty N, Mohanty P & Ghosh G (2016) *Materials Science and Engineering: C*. **65,** 269-277.
110. Ortiz Silva NA, Denis S, Vergnaud J (2024) *International Journal of Pharmaceutics* **650,** 123491.
111. Ahmad HF & Sambanis A (2013) *Acta Biomater.* **9(6)**, 6814-6822.
112. Murua A, Orive G, Hernández RM & Pedraz JL (2009) *Biomaterials* **30(20),** 3495-501.
113. Cagol N, Bonani W, Maniglio D, Migliaresi C & Motta A (2018) *Tissue Eng Part C Methods* **24(1),** 20-31.
114. Camboni A, Van Langendonckt A, Donnez J, Vanacker J, Dolmans MM & Amorim CA (2013) *Cryobiology* **67(1),** 64-69.
115. Massie I, Selden C, Morris J, Hodgson H & Fuller B (2011) *CryoLetters* **32(2),** 158-165.
116. Mahler S, Desille M, Frémond B, Chesné C, Guillouzo A, Campion JP, et al. (2003) *Cell Transplant.* **12(6),** 579-592.
117. Tan J, Jia S, Xu Q, Lin C, Cao Y, Shen J, et al. (2024) *Colloids and Surfaces B: Biointerfaces* **242,** 114096.
118. Paz-Artigas L, Ziani K, Alcaine C, Báez-Díaz C, Blanco-Blázquez V, Pedraz JL, et al. (2021) *International Journal of Pharmaceutics* **607**, 121014.
119. Malpique R, Osório LM, Ferreira DS, Ehrhart F, Brito C, Zimmermann H, et al. (2009) *Tissue Engineering Part C: Methods* **16(5)**, 965-977.
120. Serra M, Correia C, Malpique R, Brito C, Jensen J, Bjorquist P, et al. (2011) *PLoS One* **6(8),** e23212.
121. Yu J, Pan P, Li X, Zhang J, Dingzhang X, Jiang X, et al. (2025) *Biomacromolecules* **26(11),** 7289-99.
122. Umemura E, Yamada Y, Nakamura S, Ito K, Hara K & Ueda M (2011) *Tissue Eng Part C, Methods* **17(8),** 799-807.
123. Huang H, Choi JK, Rao W, Zhao S, Agarwal P, Zhao G, et al. (2015) *Advanced Functional Materials* **25(44),** 6939-6950.
124. Sevenler D, Bean H, Toner M & Sandlin RD (2021) *Cryobiology* **103,** 150-152.

125. Trufanova N, Hubenia O, Kot Y, Trufanov O, Kovalenko I, Kot K, et al. (2025) *Biopreserv and Biobanking* **23(5),** 431-438.
126. Xiang X, Liu Z & Zhao G. (2020) *Biopreservation and Biobanking* **18(4),** 321-328.
127. Passanha FR, Gomes DB, Piotrowska J, Moroni L, Baker MB & LaPointe VLS (2022) *J Tissue Eng Regen Med*. **16(1),** 14-25.
128. Touani FK, Hamouda I, Noiseux N, Hoesli C, Der Sarkissian S & Lerouge S (2025) *Biomedical Materials* **20(1)**, 015041.
129. Cao K, Shen L, Guo X, Wang K, Hu X, Ouyang X, et al. (2020) *Biopreservation and Biobanking* **18(3),** 228-234.
130. Lu HF, Narayanan K, Lim S-X, Gao S, Leong MF & Wan ACA (2012) *Biomaterials* **33(8),** 2419-2430.
131. Massie I, Selden C, Hodgson H & Fuller B (2013) *Tissue Eng Part C, Methods* **19(3),** 189-195.
132. Magalhães R, Anil Kumar PR, Wen F, Zhao X, Yu H & Kuleshova LL (2009) *Biomaterials* **30(25),** 4136-4142.
133. Magalhães R, Wang XW, Gouk SS, Lee KH, Ten CM, Yu H, et al. (2008) *Cell Transplant.* **17(7)**, 813-828.
134. Tan FC, Lee KH, Gouk SS, Magalhaes R, Poonepalli A, Hande MP, et al. (2007) *CryoLetters* **28(6),** 445-460.
135. Kuleshova LL, Tan FC, Magalhães R, Gouk SS, Lee KH & Dawe GS (2009) *Cell Transplant.* **18(2),** 135-144.
136. Wu Y, Wen F, Gouk SS, Lee EH & Kuleshova LL (2015) *CryoLetters* **36(5),** 325-335.
137. Bhakta G, Lee KH, Magalhães R, Wen F, Gouk SS, Hutmacher DW, et al. (2009) *Biomaterials* **30(3),** 336-343.
138. Kuleshova LL, Wang XW, Wu YN, Zhou Y, Yu H (2004) *CryoLetters* **25(4),** 241-254.
139. Wu Y, Yu H, Chang S, Magalhães R & Kuleshova LL (2007) *Tissue Eng.* **13(3),** 649-658.
140. Mukherjee N, Chen Z, Sambanis An & Song Y (2005) *Cell Transplant*. **14(7),** 449-456.
141. Song YC, Chen ZZ, Mukherjee N, Lightfoot FG, Taylor MJ, Brockbank KG, et al. (2005) *Transplant Proc.* **37(1),** 253-255.
142. Zaikov V, Petrenko Y, Trufanova NA, Pravdyuk A, Volkova N, Mazur S, et al. (2014) *Problems of Cryobiology and Cryomedicine* **24,** 222-230.
143. Trufanova NA, Zaikov VS, Zinchenko AV, Petrenko AY & Petrenko YA (2016) *CryoLetters* **37(6),** 440-447.
144. Pu Z, Zhang L, Yang H, Shao T, Wang D, Wang J, et al. (2025) *International Journal of Biological Macromolecules* **296,** 139716.
145. Li Y, Memon K, Zheng Y, Cheng Y, Mbogba MK, Wang P, et al. (2019) *ACS Biomaterials Science & Engineering* **5(10),** 5273-5283.
146. Zhang W, Yang G, Zhang A, Xu LX & He X (2010) *Biomedical Microdevices* **12(1),** 89-96.
147. Ekpo MD, Boafo GF, Yang Y, Seid Y, Chen C, Tan S, et al. (2025) *Macromolecular Bioscience* **2025**, e00217.
148. Meiser I, Majer J, Katsen-Globa A, Schulz A, Schmidt K, Stracke F, et al. (2021) *Cryobiology* **103**, 57-69.
149. Ladeira BM, Custódio CA & Mano JF (2022) *Biomaterials Science* **10(9)**, 2122-2153.
150. Cui Y, Nash AM, Castillo B, Sanchez Solis LD, Aghlara-Fotovat S, Levitan M, et al. (2022) *Cellular and Molecular Bioengineering* **15(5)**, 425-437.
151. Khayyat D, Glasmacher B & Gryshkov O (2021) in *SPhERe – Proceedings of the 4th International Symposium on Pharmaceutical Engineering Research –S*, pp 28-31.
152. Li C, Liu J, Wu Q, Chen X & Ding W (2021) *Chinese Journal of Chemical Engineering* **33**, 249-255.
153. Qin X, Chen Z, Shen L, Liu H, Ouyang X & Zhao G (2023) *Nano-Micro Letters* **16(1),** 3.
154. Lu YC, Fu DJ, An D, Chiu A, Schwartz R, Nikitin AY, et al. (2017) *Adv Biosyst.* **1(12),** 201700165.
155. Tang Z, Wang Y, Yang Z, Chen J, Cai S, Zhang Z, et al. (2025) *Regen Ther.* **30,** 1052-61.
156. Pruß D, Oldenhof H, Wolkers WF & Sieme H (2022) *Animal Reproduction Science* **238**, 106945.
157. Yao J, Shen L, Chen Z, Zhang B & Zhao G (2022) ACS *Biomaterials Science & Engineering* **8(5),** 2066-75.
158. Zhao G, Liu X, Zhu K & He X (2017) *Adv Healthcare Mater.* **6(23),** 1700988.
159. Song T & Liu B (2024) *CryoLetters* **45(2),** 114-21.

160. Cao Y, Zhao G, Panhwar F, Zhang X, Chen Z, Cheng L, et al. (2019) *Adv Mater Technol*. **4(1),** 1800289.
161. Tian C, Zhang X & Zhao G (2019) *Biomaterials Science* **7(3),** 889-900.
162. Kofron MD, Opsitnick NC, Attawia MA & Laurencin CT (2003) *Journal of Orthopaedic Research* **21(6),** 1005-1010.
163. Liu BL, McGrath J, McCabe L & Baumann M (2002) *Cell Preservation Technology* **1(1)**, 33-44.
164. Kubo K & Kuroyanagi Y (2005) *Artificial Organs* **29(10),** 800-805.
165. Teo KY, DeHoyos TO, Dutton JC, Grinnell F & Han B (2011) Biomaterials **32(23)**, 5380-90.
166. Bernemann I, Manuchehrabadi N, Spindler R, Choi J, Wolkers WF, Bischof JC, et al. (2010) *CryoLetters* **31(6),** 493-503.
167. Petrenko YA, Petrenko AY, Martin I & Wendt D (2017) *Cryobiology* **76,** 150-153.
168. Farooque TM, Chen Z, Schwartz Z, Wick TM, Boyan BD & Brockbank KG (2009) *Bioprocessing* **8(4),** 29-36.
169. Chinnasami H, Dey MK & Devireddy R (2023). *Bioengineering* **10(7),** 759.
170. Cornelissen M & Lippens E (2010) *Cells Tissues Organs* **192(3),** 177-186.
171. Katsen-Globa A, Meiser I, Petrenko YA, Ivanov RV, Lozinsky VI, Zimmermann H, et al. (2014) *Journal of Materials Science*: *Materials in Medicine* **25(3),** 857-871.
172. Liu B, McGrath J, McCabe L & Baumann M (2006) *African Journal of Biotechnology* **5(21),** 2014-2019.
173. Matsumura Y, Ujihira M, Nogawa S, Kimura K, Ichikawa H & Mabuchi K (2007) *CryoLetters* **28(5),** 337-346.
174. Mutsenko VV, Gryshkov O, Lauterboeck L, Rogulska O, Tarusin DN, Bazhenov VV, et al. (2017) *Int J Biol Macromol*. **104(B),** 1955-1965.
175. Tam E, McGrath M, Sladkova M, AlManaie A, Alostaad A & de Peppo GM (2020) *Annals of the New York Academy of Sciences* **1460(1),** 77-87.
176. Rogulska O, Tykhvynska O, Revenko O, Grischuk V, Mazur S, Volkova N, et al. (2019) *Stem Cells International* **2019**, 4150690.
177. Higgins AZ & Karlsson Jens OM (2013) *Biophysical Journal* **105(9),** 2006-2015.
178. Irimia D & Karlsson JOM (2002) *Biophysical Journal* **82(4),** 1858-1868.
179. Yang L, Sun H-Y, Qi N-M & Tan W-S (2012) *Biotechnology and Bioprocess Engineering* **17(1),** 195-202.
180. Hernández-Tapia LG, Fohlerová Z, Žídek J, Alvarez-Perez MA, Čelko L, Kaiser J, et al. (2020) *Materials (Basel, Switzerland)* **13(8)**, 1966.
181. Leppik L, Gempp A, Kuçi Z, Kuçi S, Bader P, Bönig H, et al. (2022) *Int J Mol Sci.* 23(3), 1425.
182. Simitzi C, Zhang J, Marksteiner R, Fuller B & Day RM (2025) *Cytotherapy* **27(12)**, 1471-1483.
183. Herrero-Gómez A, Azagra M & Marco-Rius I (2022) *Biomedical Materials (Bristol, England)* **17(4)**, 045023.
184. Kumari J & Kumar A (2017) *Scientific Reports* **7(1),** 41551.
185. Yin H, Cui L, Liu G, Cen L & Cao Y ((2009) *Cryobiology* **59(2),** 180-187.
186. Wang Z, Qing Q, Chen X, Liu C-J, Luo J-C, Hu J-L, et al. (2016) *Applied Surface Science* **388**, 223-227.
187. Dahl SL, Chen Z, Solan AK, Brockbank KG, Niklason LE & Song YC (2006) *Tissue Eng.* **12(2),** 291-300.
188. Trufanova N, Kovalenko I & Petrenko O (2020) *Problems of Cryobiology and Cryomedicine* **30(1),** 77-89.
189. Steif PS, Palastro M, Wan CR, Baicu S, Taylor MJ & Rabin Y (2005) *Cell Preserv. Technol.* **3(3),** 184-200.
190. Fahy GM, Wowk B, Wu J & Paynter S (2004) *Cryobiology* **48(1),** 22-35.
191. Warner RM, Brown KS, Benson JD, Eroglu A & Higgins AZ (2022) *Cryobiology* **108,** 1-9.
192. Acker JP, Larese A, Yang H, Petrenko A & McGann LE (1999) *Cryobiology* **38(4)**, 363-371.
193. Taylor MJ, Solanki PK, Chen Z, Baicu S, Crossley C, Greene ED, et al. (2024) *Cryobiology* **117,** 104976.
194. Cao Y, Hassan M, Cheng Y, Chen Z, Wang M, Zhang X, et al. (2019) *ACS Applied Materials & Interfaces* **11(13),** 12379-12388.
195. Gangwar L, Han Z, Scheithauer C, Namsrai B-E, Kantesaria S, Goldstein R, et al. (2025) *Nature Communications* **16(1),** 8511.
196. Kuleshova L & Hutmacher D (2008) in *Tissue Engineering*, (eds) Blitterswijk CV, Thomsen P, Lindahl A, Hubbell J, Williams

DF, Cancedda R, et al., Academic Press, Burlington, pp. 363-401.
197. Kleinhans FW, Seki S & Mazur P (2010) *Cryobiology* **61(2)**, 231-233.
198. Matsumura K, Hatakeyama S, Naka T, Ueda H, Rajan R, Tanaka D, et al. (2020) *Biomacromolecules* **21(8)**, 3017-3025.
199. Etheridge ML, Xu Y, Choi J & Bischof JC (2013) *Cryobiology* **67(3),** 398-399.
200. Xu R, Brookshaw T, Erro E, Selden C & Martin E (2025) *Sci Rep* **15,** 37664.
201. Filz von Reiterdank I, Dinicu AT, Rosales I, Cetrulo CL, Coert JH, Mink van der Molen AB, et al. (2024) *Scientific Reports* **14(1),** 22339.
202. Emteborg H & Charoud-Got J (2024) *Applied Sciences* **14(7)**, 22339.
203. Egorikhina MN, Rubtsova YP, Linkova DD, Charykova IN, Farafontova EA & Aleinik DY (2024) *Polymers* **16(2),** 247.
204. Massie I, Selden C, Hodgson HJF & Fuller BJ (2012) *Tissue Engineering Part C, Methods* **19(3),** 189-195.
205. Gryshkov O, Pogozhykh D, Hofmann N, Pogozhykh O, Mueller T & Glasmacher B (2014) *PLoS One* **9(9),** e107911.
206. Livingston DP (2018) in *Survival Strategies in Extreme Cold and Desiccation: Adaptation Mechanisms and Their Applications* (eds) Iwaya-Inoue M, Sakurai M & Uemura M, Springer Publishing, Singapore, pp. 117-127.
207. Kovalov GO, Shustakova GV, Gordiyenko EY, Fomenko YV & Glushchuk MI (2021) *Cryobiology* **103**, 32-38.
208. Kovalov GO, Chyzh MO, Globa VY, Todrin OF, Shustakova GV, Gordiyenko EY, et al. (2025) *Cryobiology* **120,** 105259.
209. Lietta E, Colucci D, Distefano G & Fissore D (2009) *Journal of Pharmaceutical Sciences* **108(1),** 391-398.
210. Warburton L & Rubinsky B (2023) *Gels* **9(6)**, 502.
211. Zaragotas D, Liolios NT & Anastassopoulos E (2016) *Cryobiology* **72(3)**, 239-243.
212. Daily MI, Whale TF, Kilbride P, Lamb S, John Morris G, Picton HM, et al. (2023) *Journal of The Royal Society Interface* **20(199),** 20220682.
213. Daily MI, Whale TF, Partanen R, Harrison AD, Kilbride P, Lamb S, et al. (2020) *Cryobiology* **93**, 62-69.
214. Zhang X, Zhao G, Cao Y, Haider Z, Wang M & Fu J (2018) *Biomater Sci.* **6(12),** 3139-3151.
215. Mutsenko V, Anastassopoulos E, Zaragotas D, Simaioforidou A, Tarusin D, Lauterboeck L, et al. (2023) *Cryobiology* **111,** 57-69.
216. Beheshtizadeh N, Gharibshahian M, Pazhouhnia Z, Rostami M, Zangi AR, Maleki R, et al. (2022) *Biomedicine & Pharmacotherapy* **153,** 113431.
217. Yusuf S, Hay E & Sansoucy E (2024) The commercialization of tissue engineered medical products: Challenges and recommendations. *World Journal of Advanced Research and Reviews* **23(02)**, 1203-1212.
218. Jitraruch S, Dhawan A, Hughes RD, Filippi C, Soong D, Philippeos C, et al. (2014) *PLoS One* **9(12),** e113609.
219. Dhawan A, Chaijitraruch N, Fitzpatrick E, Bansal S, Filippi C, Lehec SC, et al. (2020) *Journal of Hepatology* **72(5)**, 877-884.
220. Měřička P, Jandová M, Gregor J, Paterová P, Rudolfová Š, Navrátil Jr P, et al. (2025) *CryoLetters* **46(5),** 286-300.
221. Toner M & Kocsis J (2002) *Ann N Y Acad Sci*.**961,** 258-262.
222. Mahajan A, Leone R & Hubel A (2025) *Cell & Gene Therapy Insights* **11(5),** 635–645.
223. Niebergall-Roth E & Kluth MA (2025) *Journal of Translational Medicine* **23(1),** 932.
224. Awan M, Erro E, Forster-Brown E, Brookshaw T, Chandel S, Chalmers S-A, et al. (2022) *Cryobiology* **106,** 79-83.
225. Wang Y, Yang K, Yuan S, Huo F, Yang C & Tian W (2026) *Frontiers in Bioengineering and Biotechnology* **14**, 1717539.
226. Guadix JA, López-Beas J, Clares B, Soriano-Ruiz JL, Zugaza JL & Gálvez-Martín P (2019) *Pharmaceutics* **11(11),** 552.
227. Joyce K, Buljovcic Z, Rosic G, Kaszkin-Bettag M & Pandit A (2023) *Tissue Engineering Part B, Reviews* **29(1),** 78-88.
228. Becker F, Martins S, Hernandez-Bautista CA, Greber B, Zweigerdt R & Kogler G (2026) *Scientific Reports* **16(1),** 1640.
229. Martins F & Ribeiro MHL (2025) *Stem Cell Reviews and Reports* **21(3),** 645-679.
230. Uno Y, Hayashi Y, Sugiyama H, Okuda J, Nakamura T & Kino-oka M (2026) *Biotechnology Advances* **87,** 108763.
231. Gangwar L, Han Z, Scheithauer C, Namsrai BE, Kantesaria S, Goldstein R, et al. (2025) *Nature Commun* **16,** 8511.

232. Pan J, Zeng Q, Peng K, Zhou Y & Shu Z (2023) *Biopreservation and Biobanking* **22(4),** 304-311.
233. Bock A-K, Ibarreta D & Rodriguez-Cerezo E (2003) *Human Tissue Engineered Products : Today's Markets And Future Prospects*, Technical Report Series, Institute for Prospective Technological Studies & European Science and Technology Observatory & EU Commission, 62 pp.
234. Lu L, Arbit HM, Herrick JL, Segovis SG, Maran A & Yaszemski MJ (2015) *Ann. Biomed. Eng.* **43(3),** 796-804.
235. Perin F, Ouyang L, Lim KS, Motta A, Maniglio D, Moroni L, et al. (2026) *Advanced Materials* **38(4)**, e04037.
236. Sekar MP, Budharaju H, Zennifer A, Sethuraman S, Vermeulen N, Sundaramurthi D, et al. (2021) *J. Tissue Eng.* **12,** 20417314211027677.
237. Cobb H, Aparicio-Domingo S & Canto-Soler MV (2021) *Translational Vision Science & Technology* **10(10),** 9.